UNIVERSITY OF HELSINKI REPORT SERIES IN PHYSICS

HU-P-D87

SAXS STUDIES ON IONOMERS AND POLYMER–AMPHIPHILE COMPLEXES

Mika Torkkeli

Department of Physics
Faculty of Science
University of Helsinki
Helsinki, Finland

ACADEMIC DISSERTATION
To be presented, with the permission of
the Faculty of Science of the University of Helsinki,
for public criticism in Auditorium F-I of
the Department of Physics on December 16 th, 2000, at 12 o'clock.

Helsinki 2000

ISBN 951-45-8944-0
ISBN 952-91-2887-8 (pdf version)
ISSN 0356-0961
Tummavuoren kirjapaino
Vantaa 2000

Preface

This thesis is based on the research done at the X-Ray Laboratory of the Department of Physics, University of Helsinki. I wish to thank Professors Juhani Keinonen, Mauri Luukkala and Kaarle Kurki-Suonio for the opportunity to work at the Department of Physics. Professors Timo Paakkari and Seppo Manninen as laboratory chairmen I thank for placing the facilities at my disposal and setting a loose and relaxed working atmosphere.

The work has been conducted in part while the author was a member of the National Graduate School in Materials Physics.

I am grateful to my supervisor Docent Ritva Serimaa for her advice and guidance during my career and also for critical comments on the manuscript. Dr Sakari Vahvaselkä I could always rely on experimental advice. Thanks are also due to the technical staff, Messrs. Matti Laitinen, Pekka Pihkala and Raimo Jouhten.

This work would not exist without the scientific interest and ambition of the many research groups responsible for the adjoining publications. Dr Mikael Paronen and Professor Franciska Sundholm are thanked for disposing the polymer samples in Paper I for my use. DI Juha Merta and Professor Per Stenius have contributed significantly to Paper II and I have benefited greatly on their expertise in surfactant chemistry. Foremost, to Professor Olli Ikkala, Dr Janne Ruokolainen and Professor Gerrit ten Brinke I owe the credit of Papers III-V and countless others. I should thank several coworkers including MSc Juha Tanner, Dr Terhi Vikki, MSc Riikka Mäki-Ontto *nee* Mäkinen and Dr Sami Hietala for their input in this work. Special thanks to Dr Mika Saariaho and Dr Cor Luyten for company during dull work at the beamlines, home and abroad. The staff of beamline 8.2 in Daresbury and beamlines B1 (JUSIFA) and A2 (POLYP) at Hamburg are acknowledged for support in the experiments carried out there.

The personnel of the x-ray laboratory is thanked, as a whole, for being a constant source of advice and trivia. MSc Kaija Jokela, MSc Minna Toivonen and Mr Teemu Ikonen have made some of the measurements that I was able to present in this thesis. The help of Dr Veli Eteläniemi was invaluable in carrying out the experiments and preparing manuscript to Paper I.

My deepest gratitude I owe to my spouse Marja for her companionship during the few off-hours.

Helsinki, 14th November 2000

Mika Torkkeli

M. Torkkeli: SAXS Studies on Ionomers and Polymer-Amphiphile Complexes, University of Helsinki, 2000, 62 p.+appendices, University of Helsinki, Report Series in Physics, HU-P-D87, ISSN 0356-0961, ISBN 951-45-8944-0.

Classification (INSPEC): A6110F, A6140K
Keywords: x-ray scattering, polymer structure, surfactants

Abstract

In recent years there has been growing interest in extending the traditional use of polymers by attaching into them functional side groups. Side groups can influence the materials properties in a very subtle way by controlling the crystallinity of the product or by inducing a totally different kind of organization by their mesogenic property. The side groups are either covalently grafted into polymer chain or held in place by secondary physical interactions.

One area of research has been to prepare electrically conducting polymeric materials. Most studied in this field are perfluorinated ionomers. This work describes another type of conducting polymer obtained by grafting poly(vinylidene fluoride) (PVDF) films with sulfonated polystyrene (PSS).

The major part of the thesis is devoted to studies of mesoscopic phases formed by polymers, when they interact with surfactant side groups. The concept is then similar to side chain liquid crystal polymers (SCLCP's) except the interaction with the side group is non-covalent. Cationic starch (CS) is an example of polyelectrolyte. It's structure formed with anionic surfactants is investigated. Poly(4-vinyl pyridine) (P4VP) is an electrically neutral, flexible polymer. It is rendered mesoscopic by interaction with surfactants ranging from ionic to hydrogen bonding. When part of a polymer block, they exhibit two-level self-assembly akin to liquid crystalline block copolymers.

The method of investigation that is concerned here is small angle x-ray scattering (SAXS). It is particularly suitable in studying bulk properties and density-density correlations within size range 10–1000 Å. Both conventional source and synchrotron radiation are applied.

Contents

List of papers

This thesis consists of an introductory part followed by five research papers.

I M. Torkkeli, R. Serimaa, V. Eteläniemi, M. Toivola, K. Jokela, M. Paronen and F. Sundholm, *ASAXS Study of Styrene-Grafted Sulfonated Poly(vinylidene fluoride) Membranes*, J.Polym.Sci. Part B: Polym.Phys. **38** (2000) 1734-48.

II J. Merta, M. Torkkeli, T. Ikonen, R. Serimaa and P. Stenius, *The Structure of Cationic Starch (CS) / Anionic Surfactant Complexes Studied by Small Angle X-ray Scattering (SAXS)*, manuscript submitted.

III J. Ruokolainen, M. Torkkeli, R. Serimaa, S. Vahvaselkä, M. Saariaho, G. ten Brinke and O. Ikkala, *Critical Interaction Strength for Surfactant-Induced Mesomorphic Structures in Polymer-Surfactant Systems*, Macromolecules **29** (1996) 6621-6628.

IV J. Ruokolainen, M. Torkkeli, R. Serimaa, B.E. Komanschek, O. Ikkala and G. ten Brinke, *Order-Disorder Transitions in Polymer-Surfactant Systems*, Phys. Rev. E **54**, (1996) 6646-6649.

V J. Ruokolainen, M. Saariaho, O. Ikkala, G. ten Brinke, E. Thomas, M. Torkkeli and R. Serimaa, *Supramolecular Routes to Hierarchial Structures: Comb-Coil Diblock Copolymers Organized with Two Length Scales*, Macromolecules **32** (1999) 1152-1158.

Introduction

This thesis wraps up some of the experience by the author in the field of small angle x-ray scattering (SAXS). It has evolved around application to polymeric materials for the fact that it is in this field that this slightly dormant technique has regained attention during the past 5-10 years. SAXS at some stage was considered waning science incapable of competing with the much more detailed information obtained in *e.g.* electron microscopy and electron diffraction and not as powerful anyway as neutron scattering. Still x-rays struggle on and SAXS remains a standard tool of structure characterization. This is in part due to it's availability; a simple laboratory equipment such as used in this thesis is a low budget apparatus compared to its competitors. At the same time, synchrotron radiation facilities have raised the power of x-rays to a completely new level. By increasing demand, more and more beamlines are dedicated to the SAXS technique.

A second factor favoring this technique is the increase in interest toward *soft condensed matter*. This type of substance incorporates large groups of molecules held together with interactions, as in polymers, colloids or surfactant micelles to give a few examples. They are generally called *mesoscopic* ('medium sized'), therefore quite conveniently organize at length scales that are reached in SAXS measurements. By their materials property, the soft matter occupies sort of middle region between fluids (liquids) and solids (crystals). Being assemblies of many molecules the groups form thermodynamic ensembles, yet they are small enough for fluctuation effects within them to become important. This gives extra value for the statistical information on a large number of these groups as is obtained in an x-ray scattering experiment. Being sometimes very viscous fluids these new materials are also quite difficult to prepare for direct imaging with electron microscope.

This thesis is arranged as follows. It deals with concentrated system of particles and a brief account on scattering theory for such systems is given. Particular weight is given to properties of surfactant micelles as they also form the structural basis for the polymer morphologies which are studied in the research papers. Polymer/amphiphile and block copolymer behavior is understood from earlier work done on surfactant/water systems so it seems fair that a detailed presentation of surfactants and micelles is given. Application to polymers is postponed until the final chapters of this introduction.

Method

Word-for-word, SAXS defines only an angular region of scattering of x-rays, so why consider it as a separate technique? Historically, the word has been attached to the powerful scattering halo that was observable in the x-ray photographs at very small angles.[1] In due course experimentalists realized that the halo was caused by scattering of tiny particles [1], and the average size of the particles could be derived from the extent of the corona by the beam stop. This, albeit they could not agree whether the effect was actually due to refraction or diffraction [2]. The sizes of small dissolved molecules were determined already in the late 20's by considering them as "dielectric spheres of uniform optical quality" in analogy of optical scattering [3].

Among these early studies, the particular scattering properties of surfactants

[1] Though known in less complimentary terms as it was considered something of a nuisance.

were already acknowledged [4]. Krishnamurti [5] had observed powerful small angle scattering from liquid mixtures and colloidal solutions such as Sodium Oleate, a substance which is also studied in paper II of this thesis.

Thus SAXS is traditionally understood as particle scattering. However, as the previous paragraph tells, ordered structures were studied early on. This thesis and all the papers herein also study ordered structures. In this respect the technique does not earn a separate name as it is basically powder diffraction performed at small angles because of the large size of the crystalline unit cells. The distinction is more in the experimental size. In SAXS, a relatively weak intensity is measured close to the primary beam. Whence, it requires a different sort of apparatus with a very finely collimated beam. On the other hand, the geometry of the experiment is much simplified from wide angle scattering (WAXS) and most corrections made in WAXS reduce to unity because of small angles.

Basic SAXS properties

We consider here static elastic scattering of x-rays which are very short wavelength electromagnetic waves. The word 'static' means that the matter is viewed as frozen[2] during the time it takes for the packet of plane wave, photon, to enter and leave the sample. 'Elastic' means that the diffracted wave (or re-emitted photon) has the same wavelength (energy) as the incident wave. The incident and scattered waves, denoted by wave vectors $\mathbf{k}_1$ and $\mathbf{k}_2$, then have the same magnitude $2\pi/\lambda$, where λ is the wavelength.

The scattering is due to electrons, each of which emits radiation with a fixed phase difference to the incident radiation (barring dispersion effects). Then the relative phase of the scattered wave depends only on the position of the electron through $\mathbf{r}$ as $\mathbf{k} \cdot \mathbf{r}$, where $\mathbf{k} = \mathbf{k}_2 - \mathbf{k}_1$ is the so called scattering vector. Note that this product in general reflects the reciprocal relation between the size and the scattering angle. The magnitude of the scattering vector k is given by the scattering angle 2θ as

$$k = 4\pi \sin\theta/\lambda. \tag{1}$$

The type of information usually obtained in SAXS is exemplified by the two most basic laws. In the late thirties, André Guinier considered the limiting form of scattering intensity at very small angles for a system of independently scattering particles [6]. The intensity always shows a decreasing slope whose steepness determines how far on average the particle extends from its center of gravity — it's radius of gyration. The second traditional application roots from the large angle scattering behavior. At this extreme the scattering is sensitive to the surface regions. It was left to Porod [7] to formulate the law that the scattering from a two phase structure with sharp boundaries is proportional to the surface area and the inverse of the fourth power of the scattering vector k^{-4}. Lately, this observation has been extended on systems with different dimensionality leading to a similar scaling law of the intensity curve [8].

[2] The term "time resolved scattering" may emerge in some articles but is not meant to deal with time correlations related to dynamic properties of the scattering media, though made possible by synchrotron radiation. These refer quite simply to the changes in the static structure factor with time as sample circumstances (*i.e.* temperature) is changed.

Experimental

The requirements for a small angle x-ray scattering setup can be listed very briefly. The objective is to obtain high flux and sufficiently small cross-section of the beam at the detector position. The beam size defines the *angular resolution* of the device and it is reduced using slit collimation or focusing devices such as curved monochromators and mirrors. However, of equal importance is to guard the detector from the parasitic scattering which inevitably arises from the collimation. This background chiefly limits *the smallest achievable angle*. The simplest configuration uses slit collimation. The angular resolution is controlled by choosing appropriate apertures. There is quite an unfavorable trade-off between resolution and intensity, at worst six orders orders of magnitude decrease in intensity for an order of magnitude increase in resolution. Focusing optics can significantly increase the obtained flux. However, one can expect increased background level from the focusing optics as compared to slit collimation.

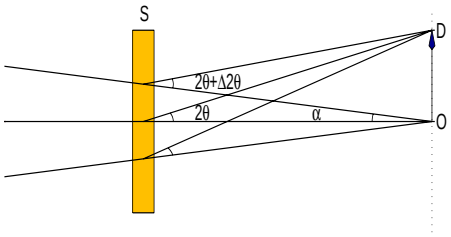

Figure 1: SAXS geometry. The rays are scattered by a flat specimen (S) placed normal to the beam and measured at position (D) at the plane of detection (dotted line). The scattering angle 2θ is approximately given by the distance OD divided by sample to detector distance SO. Rays with different angle of incidence α (beam divergence) will induce a relatively small error $\Delta 2\theta / 2\theta \approx \alpha(2\theta - \alpha)$

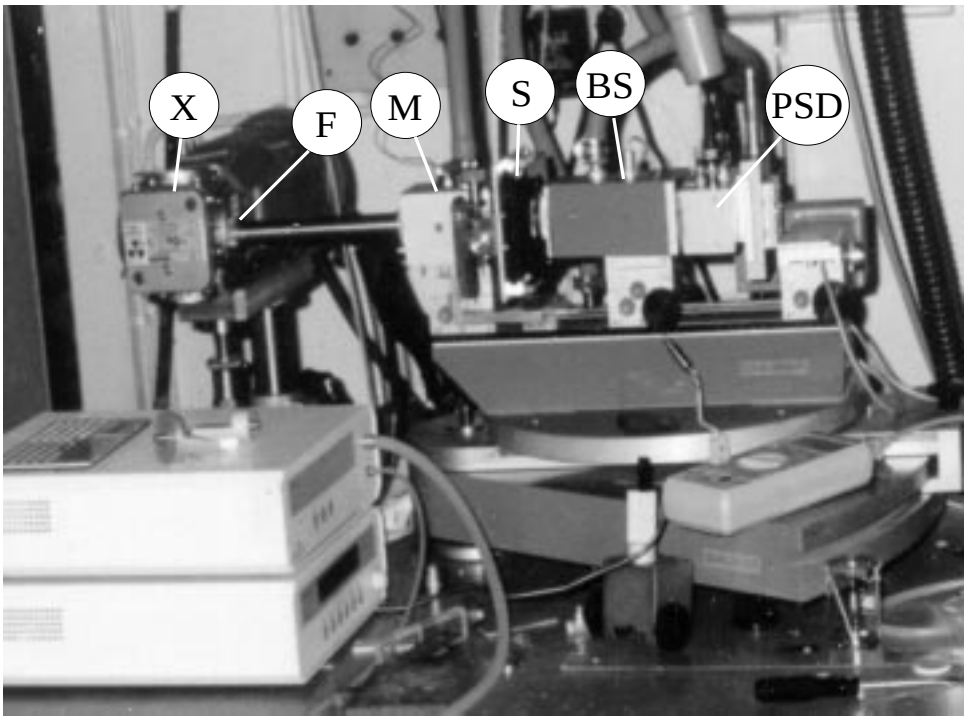

Figure 2: A SAXS workbench; Helsinki, circa 1999.

A practical SAXS setup has considerable smearing effects due to the finite beam size. Thus strict energy purity may also be thought as a waste of flux. For a conventional device, a β-filter accompanied with a high energy cutoff mirror suffices for monochromatization.

Device at HU. The small angle scattering setup at HU is pictured in Fig. 2. The device consists of a sealed Cu-anode x-ray tube (X); monochromatizer section with Ni-filter (F) at front end and a flat glass mirror (M) at the rear; temperature controlled sample stage (S); vacumized scattering path with slightly transparent beam stop (BS) and a linear position sensitive detector (PSD).

The apparatus was originally designed to be used with weakly scattering samples such as dilute solution of molecules. Therefore the system used line focusing geometry, where the beam is narrowed in one dimension only so that small angles can be reached without great loss in intensity [9]. The line profile has drawbacks in measuring intensities with sharp features. For example, well ordered structures produce diffraction maxima, which become smeared and develop a tail toward zero angle. These distortions can in principle be corrected [9, 10, 11] for which the higher statistical accuracy is of use.

To oppose the slit height smearing, the apparatus is preferably used in point focusing mode. This is not to say this is an essential step in structure determination at small angles; even Kratky cameras have been utilized without further corrections as has been demonstrated recently [12]. There are further advantages in point focusing. The beam size measures typically 0.1 x 1 mm at the sample so smaller samples and sample cells for the temperature stage are needed. Secondly, the operation of the PSD is much affected by high countrates. With the line focus, the counting capacity of the PSD (MBraun OED-50M) is easily exceeded. In changing to point focus, the intensity is lost by a factor of 50 leaving a primary flux of about $4{\cdot}10^6$ 1/s.

The resolution anomaly induced by the high count rate is easily demonstrated with a "double-slit" experiment (see Fig. 3). If two closely separated slits are placed in front of the PSD and kept open in turn, two peaks emerge at the position of the slits. However, when both the slits are open, the position signals move as if attracted toward a common center of gravity. This phenomenon is traced to space charging effects at the detector electrodes. It is particularly severe for small reflections occurring close to ($<$ 1 mm) a major peak and the minor reflections can be devoured by the major ones.

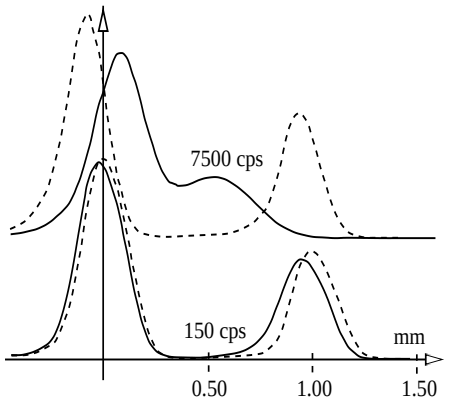

Figure 3: Position signal obtained through two slits 1 mm apart with one slit opened at a time (dashed) and with both slits open. In the lower curves the total countrate was 150 s^{-1} and in the upper curves 7500 s^{-1}

At best, high intensity produces just small offset and broadening of the position signal. Still, for high accuracy the countrates should be kept at moderate levels. A second restriction is the linearity of the detector, the so called *parallax error*. The active depth of the detector is about 5.3 mm which is substantial fraction of the standard distance between sample and detector (the camera length). To improve resolution the distance has to be increased to the point where resolu-

tion is no longer detector limited. In HU the longest camera length in use is 1165 mm. At this distance long periods over 1000 Å can be reached.

Synchrotron radiation. Synchrotron radiation (SR) is emitted by extremely fast electrons accelerating in a magnetic field. In order for the SR emission to reach the x-ray energy range, given that practical magnetic fields are limited to few Teslas, the required electron energies correspond to acceleration over 10^9 volts (GeV's). This requires large facilities which nowadays are solely dedicated to the production of SR. Electrons traveling at relativistic speeds emit radiation which is said to be naturally collimated. As such it is the perfect source for SAXS. The highest brilliancies are produced with the insertion devices. These find use in high resolution work such as very fast time resolved studies, anomalous scattering, ultra small angle scattering, surface scattering or micro-focus diffraction. For normal SAXS the intensity provided by the bending magnets is quite adequate. This is the original parasitic product of the synchrotron arising from the necessity of keeping the electrons at their circular paths. Sadly, the detectors are often not to par with the flux obtained even at the bending magnets. All SR work in this thesis is performed on beamlines utilizing bending magnets. Typical flux on sample is few hundred times that of *e.g.* the conventional source described above.

Anomalous Small Angle X-ray Scattering The atomic scattering factor does not depend just on the magnitude of the scattering vector k, but also on the energy E of the photon. The atomic scattering factor is usually expressed as a sum of three terms

$$f(k, E) = f_0(k) + f'(E) + if''(E). \tag{2}$$

These *dispersion effects* become significant when E is close to the ionization energy of the element (see Fig. 4). Far away from this edge, the scattering factor approaches f_0, which in SAXS is practically equal to the number of electrons Z within the element.

The scattering factor bears relation to the complex index of refraction n [13, p.139]

$$n = 1 - \delta - i\beta. \tag{3}$$

The real part of f is proportional to the real part of the refraction index by

$$\delta = \frac{N\lambda^2 r_e}{2\pi}(Z + f'), \tag{4}$$

where $r_e = 2.81793$ fm is the classical radius of the electron and N is the number density of the atoms. The deviation of n from unity is small, for a rough numerical estimate

$$\delta \approx 1.3 \cdot 10^{-6} \times \rho \left[\frac{\mathrm{g}}{\mathrm{cm}^3}\right] \lambda^2 \left[\mathrm{\AA}^2\right]. \tag{5}$$

The imaginary part f'' is related to the imaginary part of the refraction index,

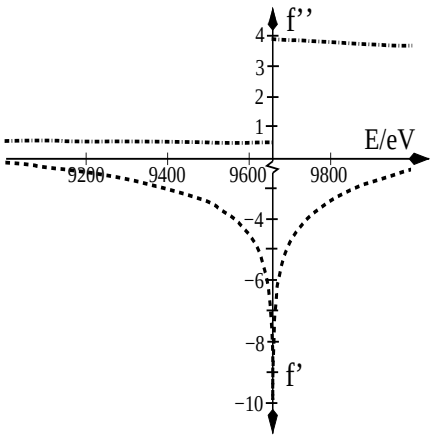

Figure 4: Dispersion correction for the scattering factor of zinc ($Z = 30$) around its K-absorption edge 9659 eV. [15]

i.e. the *linear absorption coefficient* μ by

$$\mu(=\frac{4\pi\beta}{\lambda}) = 2N\lambda r_e f''. \tag{6}$$

The terms f' and f'' are further connected by the Kramers and Kronig relation [14]

$$f'(E) = \frac{2}{\pi}\int_0^\infty \frac{\varepsilon f''(\varepsilon)}{E^2-\varepsilon^2}\mathrm{d}\varepsilon \tag{7}$$

Thus measuring the absorption spectrum gives directly the imaginary part of the scattering factor and evaluation of the dispersion integral (7) yields f'. The real part can also be measured directly by virtue of the refractive properties of the matter. Computer programs exist for calculation of the scattering factor. For example, the data in accompanying Fig. 4 is produced by the program of Brennan [15]. The calculation routines often assume a stepwise increase in f'' at the *absorption edge*. In practice the edge has a natural width which suppresses f' from approaching minus infinity. The chemical state of the element is also a very decisive factor. For some elements, the absorption spectrum shows an intense peak a.k.a. *white line* which completely obscures the absorption step.

The anomalous dispersion effect is used to derive element specific information on atom-atom distributions. The information is in the form of so-called *partial structure factors* S_{ij}, in terms of which the intensity is

$$I(k,E) = \sum_{i,j} N_i f_i(k,E) f_j^*(k,E) S_{ij}(k), \tag{8}$$

where N_i is the number of atoms of element i. The partial structure factors are related to pair distribution (correlation) functions. For homogeneous samples

$$S_{ij}(k) = \delta_{ij} + n_j \int_0^\infty 4\pi r^2 g_{ij}(r)\frac{\sin kr}{kr}\mathrm{d}r, \tag{9}$$

where n_j is the average density of element j and consequently $n_j g_{ij}(r)$ gives the density of this element at a distance r from an arbitrary atom of element i.

To obtain g_{11}, for example, three or more energies are chosen below the absorption edge of element '1' so as to induce as large a change in f_1 as possible. It is unwise to go above the edge because of the disturbing fluorescent radiation this produces. Often only one of the scattering factors can be varied significantly because of energy limitations. Therefore just three independent partial structure factors are derived from the system of equations (8). In this case, element label '2' stands for average atoms of all elements other than '1'.

In paper I, a more straightforward formula than Eq.(8) is assumed. The SAXS intensity is not pictured as arising from individual atoms, but from fluctuations in a continuous[3] variable electron density ρ_e. Acknowledging dispersion effects the variable is, precisely, scattering factor density, or *effective electron density*

$$\rho_{eff} = \rho_e + n_1(f_1' + if_1''). \tag{10}$$

[3]continuous in the resolution of SAXS experiment which is of the order of 10 Å.

If the elements are distributed homogeneously within a two phase structure, the intensity is written simply as a product of ρ_{eff}^2 and a structure factor $S(k)$, which describes the distribution of the phase regions.

Absolute Intensity Scale In some applications, *e.g.* paper I, absolute intensities are used. It is defined here by the scattered intensity per unit solid angle per unit volume per incident intensity. Detectors observe the flux of photons. At the geometry given by Fig. 1, a detector whose cross section is S and efficiency η at distance r from the sample registers flux

$$\Phi = \Phi_0 e^{-\mu t} \cdot tI \cdot \eta S \times r_e^2/r^2 \tag{11}$$

where I is the absolute intensity, Φ_0 is the incident flux, $e^{-\mu t}$ is loosely referred to as the absorption factor and t is the sample thickness. In order to get from Φ to I, the incident flux should be found out, and — depending on the method of normalization — other parameters appearing in Eq.(11).

It is most convenient if the incident flux can be obtained during the measurement. In synchrotron, where the flux varies with time, this is absolutely mandatory. If the incident flux is measured with the same detector as the scattering, by simply recording the transmitted flux $\eta\Phi_0 e^{-\mu t}$, it is not necessary to know the absorption factor and detector efficiency. However, the intense beam has to be attenuated either by filters [16] or a mechanical absorber (moving slit) [17]. The synchrotron beam is too brilliant for this. Most usually, the SR is monitored with ionization chambers before and after the sample. The beam at HU is monitored through the copper beam stop which attenuates the direct beam by a factor 7000.

One needs the least amount of information on the monitoring efficiency and measurement arrangement, if one uses reference scatterers. A *primary standard* is such for which one can predict the intensity from exact knowledge of the structure. A crystalline powder, for example silver behemate[4] might be considered. However, materials which give crystalline reflections at small angles are also keen to have texture. In SAXS it would be most natural to employ solutions of dense particles such as silica, with known size and particle density. These have the drawback that they will eventually aggregate, so new standards have to be prepared. A rare gas of simple molecules would be a reliable scatterer but unfeasible since their intensity is low. However, dense gases or simple liquids can also be employed [18]. Though the scattering involves interference between the particles, the intensity can be relied to depend on two thermodynamical properties of the standard, its isothermal compressibility χ and the number density of the molecules n

$$I(k) = F^2(k) nkT\chi \tag{12}$$

where $F(k)$ is the scattering amplitude of a single molecule. For example, the absolute intensity normalizations made at HU are relative to the scattering intensity of water [19]. According to the compressibility data, its scattering intensity at 25°C is 0.208 $1/\text{Å}^3$, *i.e.* equal to 0.208 free electrons per cubic Å.

Even liquids are impractical as standards to be measured frequently. Therefore calibrated *secondary standards* are used. A good secondary standard gives intensity curve which is strong and flat and good thermal stability is also beneficial. In HU, polyethylene (LUPOLEN) is used as a secondary standard [20]. It's intensity is again calibrated with respect to water. Glassy carbon is a second choice of standard [21], with scattering properties quite similar to LUPOLEN.

[4] Also a popular standard for calibrating the scattering vector

Scattering of non-dilute systems

A single particle does not yet provide sufficient scattering intensity. Even when studying particle scattering, the scattering cell should contain a dense collection of particles. The observed intensity then depends on the particle scattering factor $F(k)$ and the structure factor $S(k)$ associated with the distribution of the centers of particles within the media

$$I(k) = F^2(k)S(k). \tag{13}$$

It is found throughout this thesis that both $F(k)$ and $S(k)$ change appreciably within the experimental angular range. If one's interest is the particle scattering factor, one seeks to dilute the system to approach the condition of uncorrelated particles, *i.e.* $S(k)$ approaching unity. In concentrated systems, the structure factor is no longer unity but may be expressed as

$$S(k) = \int_0^\infty P(r)\frac{\sin kr}{kr}\mathrm{d}r. \tag{14}$$

This follows Debye's formulation of scattering from molecules [22]. The concept of molecule is changed into an ensemble of scattering centers and the double summation over the atoms within each molecule is replaced with a single summation over different distances between the scattering centers and the factor $P(r)$ denotes the number of such distances.

For a homogeneous density n of particles, the structure factor is alternatively expressed as

$$S(\mathbf{k}) = 1 + n\int g(\mathbf{r})e^{i\mathbf{r}\cdot\mathbf{k}}\mathrm{d}^3\mathbf{r}, \tag{15}$$

where $g(\mathbf{r})$ is the correlation function whose physical meaning is that $ng(\mathbf{r})$ is the average density of particles at position $\mathbf{r}$ from a center particle. In a small angle scattering experiment, the information about the average density is lost in the beam stop. Instead, only local density fluctuations are observed. This is effectuated by replacing $g(\mathbf{r}) \to h(\mathbf{r}) = g(\mathbf{r}) - 1$,

$$S(\mathbf{k}) = 1 + n\int h(\mathbf{r})e^{i\mathbf{r}\cdot\mathbf{k}}\mathrm{d}^3\mathbf{r} \tag{16}$$

Structure factors

If the scattering factor in Eq.(13) was known exactly, this would be of some interest, since the remaining structure factor has a relation to the interparticle potential, as we will see shortly.

The problem of finding relationship between the pair potential $V(r)$ and the correlation function $g(r)$ is ultimately linked to finding the equation of state for liquid systems. This is manifest through equations [23]

$$p = nkT - \frac{n^2}{6}\int_0^\infty 4\pi r^3 g(r)V'(r)\mathrm{d}r \quad \text{'the pressure equation'} \tag{17}$$

$$kT\left(\frac{\partial n}{\partial p}\right)_T = 1 + n\int_0^\infty 4\pi r^2\left(g(r) - 1\right)\mathrm{d}r \quad \text{'the compressibility equation'}$$

However, as we recall from statistical mechanics, the equation of state even for simple liquids can be expressed only approximately *e.g.* by the virial expansion. The two-body correlation function is coupled to all multiplet (many-body) distribution functions *ad infinitum* by a series of integral equations [24]. In the simplest case one just ignores all many particle correlations. Then the correlation function is related to the Boltzmann probability

$$g(r) \simeq e^{-\beta V(r)}. \tag{18}$$

This approximation is valid only for a very dilute system of particles. There exist a number of approximation schemes to derive structure factors of liquids in the semidilute region. They apply to volume fractions up to $\eta \approx 0.5$.

Integral methods. According to Kirkwood [25] the N particle interaction potential is expressed as sum of terms involving the pair potential

$$V_N = V_{N-1} + \xi V_1,$$

$$V_1 = \sum_{k=2}^{N} V(r_{1k}). \tag{19}$$

In this formulation particle 1 is "switched on" by parameter ξ. This approximation is known as *superposition principle*. It states that the average force acting on a third particle by two particles is the sum of individual forces without the presence of the other particle [25, 26], thus giving interparticle forces the same status as external forces.

The superposition argument reduces the problem to solving (numerically) a single integral equation [26]

$$\ln g(r,\xi) = -\beta\xi V(r) + \frac{\pi}{r}\rho \int_0^\infty \left[K(r-r',\xi) - K(r+r',\xi)\right] r' \left[g(r') - 1\right] \mathrm{d}r'. \tag{20}$$

where $g(r) \equiv g(r,1)$ and the kernel is

$$K(t,\xi) = -2\beta \int_0^\xi \mathrm{d}\xi' \int_{|t|}^\infty sV(s)g(s,\xi')\mathrm{d}s.$$

The corresponding kernel for the Born-Green-Yvon (BGY) theory is [27]

$$K(t,\xi) = \beta\xi \int_{|t|}^\infty \left(s^2 - t^2\right) V'(s)g(s,\xi)\mathrm{d}s.$$

The solution has been further simplified by Rodrigues [28] by writing the distribution as

$$g(r,\xi) = e^{-\beta\xi V(r) + f(r,\xi)}$$

The function f represents correction many-particle effects and it is therefore expected to be small. Neglecting terms f^2 and higher, the structure factor is [29].

$$S(k) = \frac{1}{1 - n\epsilon(2\pi)^{3/2} b(k)}, \tag{21}$$

where

$$b(k) = \sqrt{\frac{2}{\pi}} \int_0^\infty r^2 \left(e^{-V/kT} - 1 \right) \frac{\sin kr}{kr} \mathrm{d}r$$

and $\epsilon = f(r) + 1$ is the order of unity.

The Ornstein-Zernike equation. In 1914 L. S. Ornstein and F. Zernike were attempting to solve the problem of critical opalescence and therefore studied the properties of the correlation function near the critical point. By an ingenious insight they wrote the correlation function in a closed integral form known as the Ornstein-Zernicke (O-Z) equation [30]

$$g(r) = 1 + c(r) + n \int c(\mathbf{z}) \left[g(\mathbf{z} - \mathbf{r}) - 1 \right] \mathrm{d}\mathbf{z} \tag{22}$$

or more simply as

$$h(r) = c(r) + n \; c{*}h(r) \tag{23}$$

where $*$ denotes for convolution operation. Thus the correlation between particles is the result of direct correlation $c(r)$ and indirect correlation transmitted through the media by the same function. The wish of O&Z was that $c(r)$ would have a clear physical meaning and could be determined a priori. This was not the case and and Eq.(23) may be taken merely as its definition.

The direct correlation function is, however, a convenient concept in further approximations. It is short ranged when the potential is short ranged and vanishes where the potential is large. Once the direct correlation function is solved, the structure factor follows from the Fourier transform of the O-Z equation (16)

$$S(k) = \frac{1}{1 - nC(k)}. \tag{24}$$

For solving $c(r)$, another *closure relation* is needed to connect the direct and indirect correlation functions. Following sections give three best known examples.

Ornstein and Zernike did find an asymptotic form for $h(r)$. Developing $h(r)$ in series under the integral up to second order and noting that it is a symmetric function

$$h(r) = c(r) + h(r) \cdot n \int c(z) \mathrm{d}^3\mathbf{z} + \nabla^2 h(r) \cdot \frac{n}{6} \int z^2 c(z) \mathrm{d}^3\mathbf{z}. \tag{25}$$

At sufficiently far out $c(r) \approx 0$, and the solution satisfies

$$\left(\nabla^2 - \kappa^2 \right) h(r) = 0 \tag{26}$$

with the known solution [31]

$$h(r) = \frac{1}{4\pi n \varphi^2} \frac{e^{-\kappa r}}{r} \tag{27}$$

where

$$\kappa^2 = \frac{1 - F}{\varphi^2} \quad ; \quad F = n \int c(z) \mathrm{d}^3\mathbf{z} \quad \text{and} \quad \varphi^2 = \frac{n}{6F} \int z^2 c(z) \mathrm{d}^3\mathbf{z}.$$

This gives the O-Z structure factor [30]

$$S(k) = 1 + nH(k) = 1 + \frac{\varphi^{-2}}{\kappa^2 + k^2}. \tag{28}$$

The direct correlation function turns out to have the same form

$$c(r) = \frac{1}{4\pi n\varphi^2}\frac{e^{-qr}}{r}, \quad \text{where} \quad q^2 = \kappa^2 + \varphi^{-2}. \tag{29}$$

Mean spherical approximation. Many systems of interest have a pair potential which consists of hard-sphere interaction plus a tail. Such systems may be handled by making a *mean spherical approximation* (MSA) [32]. For the hard sphere case this is

$$\begin{array}{ll} h(r) = -1, & r < D \\ c(r) = -\beta V(r), & r > D. \end{array} \tag{30}$$

This is a first example of a closure relation to solve the O-Z equation (23). The potential at large distances is of the same exponential form (29) as $c(r)$. This is also known as the *Yukawa form*, found for *e.g.* spherical macroions in a dielectric medium. The direct correlation function for $r < D$ is also solvable [33]. The solution is referred to as the *Hayter-Penfold model* who were the first to present solution [34]

$$S(k) = \frac{1}{1 - nW(k)}. \tag{31}$$

The calculation of parameters for $W(k)$ is, however, rather lengthy, see [34, appendix A]. At the "point ion limit" $S(k)$ approaches the O-Z structure factor (28). The solution is said to have shortcomings at dilute concentrations and has later been improved by the so called *rescaled* MSA [35].

PY approximation. In 1958, Percus and Yevick proposed another closure relation [36, 37]

$$c(r) = \left[1 - e^{\beta V(r)}\right] g(r) \equiv g(r) - \tau(r). \tag{32}$$

Incredibly, this closure relation solves the O-Z equation analytically for simple hard spheres interaction, for which the O-Z equation takes form

$$\tau(r) = 1 + n\int^{r<D} \tau(z)\ \mathrm{d}^3\mathbf{z} - n\int^{\substack{z<D \\ |\mathbf{r}-\mathbf{z}|>D}} \tau(z)\ \tau(|\mathbf{r}-\mathbf{z}|)\mathrm{d}^3\mathbf{z}. \tag{33}$$

This was solved independently by Wertheim and Thiele [38]. Another case where PY closure leads to a solution is the hard-sphere potential supplemented with a short range attractive part approximated by a square well. This is known as the *sticky hard sphere model* (SHSM) of Baxter [39]. The solution takes simpler form when the structure factor is written in a factorized form [40]. Otherwise, the two models are

quite alike, so below they are presented side by side:

The hard sphere model	*The sticky hard sphere model*
$V(r) = \infty, \quad r < D$	$V(r) = \infty, \quad r < D$
$V(r) = 0, \quad r > D$	$V(r) = kT \ln 12\tau \frac{W-D}{W}, \quad D < r < W$
	$V(r) = 0, \quad r > W$
$S^{-1}(k) = 1 - nC(k)$	$S^{-1}(k) = Q(k)Q(-k)$
$C(k) = \int c(r) e^{ikr} \mathrm{d}r$	$Q(k) = 1 - 2\pi n \int q(r) e^{ikr} \mathrm{d}r$
solution :	
$-c(x) = \alpha + \beta x + \frac{\alpha\eta}{2} x^3$	$W^2 q(x) = \alpha x^2 + \beta x + (\beta - \alpha + \lambda/12)$
where $x = r/D < 1$	where $x = r/W < 1$
$\alpha = (1+2\eta)^2 / (1-\eta)^4$	$\alpha = \frac{1}{2}(1 + 2\eta - \mu)/(1-\eta)^2$
$\beta = -6\eta \left(1 + \frac{1}{2}\eta\right)^2 / (1-\eta)^4$	$\beta = \frac{1}{2}(-3\eta + \mu)/(1-\eta)^2$
parameters :	
$\eta = \frac{1}{6}\pi D^3 n$	$\eta = \frac{1}{6}\pi W^3 n$
	$\mu = \lambda\eta(1-\eta)$
	λ is the smaller root of the quadratic:
	$\tau\lambda = \frac{1}{2}\frac{2+\eta}{(1-\eta)^2} - \frac{\eta^2}{1-\eta}\lambda + \frac{\eta}{12}\lambda^2$

Parameter τ measures the 'stickiness' of the potential. Note the difference in the volume fraction parameter η. However, the solution for SHSM is strictly derived in the limit $W \to D$. Despite this unphysical aspect, the potential is successful to mimic systems with a hard core and a short range attractive potential. The SHSM has been applied for colloidal particles, microemulsion systems and nonionic micelles [41]. It also suited to model Lennart-Jones type of potential previously handled with numerical calculations [42] and predicts well the gas-liquid phase transition [43].

The structure factor for the SHSM is [44]

$$S^{-1}(k) = \left\{ 1 + 12\eta \left[2\alpha\Phi(\kappa) + \beta c(\kappa) - \frac{\lambda}{12} j_0(\kappa) \right] \right\}^2 \tag{34}$$

$$+ \left\{ \frac{12\eta}{\kappa} \left[\alpha \left(1 - 2j_0(\kappa) + 2c(\kappa)\right) + \beta \left(1 - j_0(\kappa)\right) - \frac{\lambda\kappa^2}{12} c(\kappa) \right] \right\}^2 ,$$

where $\kappa = kW$ and

$$\Phi(x) = (\sin x - x\cos x)/x^3$$
$$c(x) = (1 - \cos x)/x^2$$
$$j_0(x) = \sin x / x$$

Structure factor for the bare HSM is given by *e.g.* Kinning and Thomas [45]

$$S^{-1}(k) = 1 + 24\eta \left[(\alpha + 2\beta + 2\alpha\eta)\, \Phi(\kappa) + \beta \frac{(2+\kappa^2)\cos\kappa - 2}{\kappa^4} \right.$$

$$\left. + \frac{3}{2}\alpha\eta \left(\frac{(\kappa^4 + 6\kappa^2 - 12)\cos\kappa - 12\kappa\sin\kappa + 12}{\kappa^6} \right) \right] , \tag{35}$$

where $\kappa = kD$. Both HSM [46] and SHSM [47] have later been generalized to polydisperse mixtures, which are more appropriate for real systems.

HNC approximation. The hyper netted chain (HNC) closure is

$$\ln g(r) + \beta V(r) = h(r) - c(r). \tag{36}$$

HNC is superior to PY for long range interactions such as in ionic fluids *e.g.* electrolytes [23]. However, it is nonlinear theory and has to be solved numerically.

The benefits of HNC and PY (or MSA) schemes may also be combined by introducing a closure which mixes these two [48].

Random phase approximation. One frequently appearing concept is the *random phase approximation* (RPA), which makes use of the linear response theory. If one considers weak perturbation potential $\delta V(\mathbf{r})$, the variation in density may be approximated as [49]

$$\delta n(\mathbf{r}) = -\beta n \delta V(\mathbf{r}) - \beta n^2 \int h(\mathbf{r} - \mathbf{r}')\delta V(\mathbf{r}')\mathrm{d}\mathbf{r}'. \tag{37}$$

Fourier transform of this is

$$\delta n(\mathbf{k}) = -\beta n \delta V(\mathbf{k}) S(\mathbf{k}). \tag{38}$$

Equation (38) is, in fact, the first order Taylor series expansion of δn in powers of δV [37]. Above form is similar to O-Z Eq.(23) in that the perturbation propagates via the correlation function $h(r)$. Thus RPA is effectuated by substituting for the direct correlation function

$$c(\mathbf{r}) \to c_0(\mathbf{r}) - \beta \delta V(\mathbf{r}),$$

which gives for the structure factor

$$S(\mathbf{k}) = \frac{S_0(\mathbf{k})}{1 - nS_0(\mathbf{k})\beta V(\mathbf{k})}, \tag{39}$$

where S_0 is the unperturbed structure factor. RPA is often applied to polymers, for example for flexible polymers in solution the approximation is

$$S^{-1}(\mathbf{k}) = S_0^{-1}(\mathbf{k}) + nv, \tag{40}$$

where S_0 is the structure factor for an ideal chain and the perturbation is the excluded volume interaction which is represented here by the excluded volume v.

One dimensional substance and paracrystallinity

The exact solution for the PY closure in three dimensions is quite unique. The same method does not work in two dimensions, and one needs to resort to numerical calculations [50]. The one dimensional case —a linear chain of particles (rods) — turns out to be tractable again.

As a special case, we assume that particles interact with the nearest neighbors only.[5] The equation of state between the pressure f and the density n was obtained

[5] It suffices that the potential has a hard core and short range such that particles can never interact with the next nearest neighbors in practice.

by Takahashi during WWII [51][6]

$$n^{-1} = \frac{\int_0^\infty r \exp\left[-\beta(V(r) + fr)\right]}{\int_0^\infty \exp\left[-\beta(V(r) + fr)\right]}. \tag{41}$$

Particularly for hard rods of length L, a.k.a the Tonks gas [54]

$$f\beta = \frac{n}{1 - nL}, \tag{42}$$

which is just the ideal gas e.o.s. with the volume replaced by the free space between the rods. In Eq.(41), the pressure f acts as an external force to a bounded system of particle density n. This result applies just as well to a system of two particles and hence the quantity

$$e^{-\beta(V(r)+fr)} \tag{43}$$

is interpreted as a probability distribution for distance between neighboring particles.

It is clear that the density n is a single valued function of pressure and no phase transition is to be expected [51]. The existence of perfect periodicity in the lower dimensions have been considered very early by Peirls and Landau [55]. It is argued that thermal fluctuations prohibit perfect order when the size of the system grows without limit [56]. The one dimensional systems offer means to test this prediction. Potentials which extend beyond the nearest neighbor interaction are awkward to handle computationally [53] except for the Kac-Baker model [57]. It appears that phase transitions are possible only for potential of infinite extent.

The paracrystalline lattice. The nearest neighbor interaction leads to a distinct type of periodic system known as a *paracrystalline lattice*. The correlation function and structure factor for the one dimensional HSM was, in fact, worked out as early as 1927 by Zernike and Prins [58]. They did not need to solve the statistical mechanical "problem" to argue that the gaps between the rods follow an exponential distribution, as is evident from Eq.(43) upon insertion of the hard sphere potential. They then proceeded to calculate the structure factor using property which was later referred to as paracrystallinity by Hosemann [59].

What makes a paracrystal is that all distances between neighboring particles are independent. Thus let $p(r)$ be the probability distribution of nearest neighbor distances. Then the corresponding distribution of distances to the n-nearest neighbors follows from the n-fold convolution

$$p_n(r) = \int p_{n-1}(s)p(r - s)\mathrm{d}s. \tag{44}$$

These distributions constitute for the total correlation function [58]

$$g_1(r) = \sum_{n=-\infty}^{\infty} p_n(r). \tag{45}$$

The subscript marks that this is a one dimensional correlation function. The successive convolutions need not be worked out because by the convolution theorem

$$\phi_n(k) = \phi_{n-1}(k) \cdot \phi(k) \tag{46}$$

[6] Unaware of this, the same solution was later offered by Gursey [52] and van Hove [53].

where $\phi_n(k)$ and $\phi(k)$ denote Fourier transforms of $p_n(r)$ and $p(r)$. The structure factor is thus [59]

$$S_1(k) = 1 + \sum_{n=1}^{\infty} (\phi^n + (\phi^*)^n) = \mathrm{Re}\frac{1+\phi(\mathrm{k})}{1-\phi(\mathrm{k})}. \tag{47}$$

Few special cases may be singled out, let[7] $r = z + a$

$p(z)$	$\phi(k)$	$S_1(k)$
gaussian : $\frac{1}{\sqrt{2\pi\sigma^2}} e^{-\frac{1}{2}\frac{z^2}{\sigma^2}}$	$e^{-\frac{1}{2}\sigma^2 k^2 + ika}$	$\frac{\sinh \frac{1}{2}\sigma^2 k^2}{\cosh \frac{1}{2}\sigma^2 k^2 - \cos ka}$
exponential : $\frac{1}{c} e^{-z/c}, z > 0$	$\frac{e^{ika}}{1-ick}$	$\frac{c^2 k^2}{2+c^2 k^2 - 2\cos ka + 2ck \sin ka}$
box : $\frac{1}{2w}, \lvert z\rvert < w$	$\frac{\sin kw}{kw} e^{ika}$	$\frac{k^2 w^2 - \sin^2 kw}{k^2 w^2 - 2kw \sin kw \cos ka + \sin^2 kw}$
triangle : $\frac{1}{2w}(1 - \frac{\lvert z\rvert}{2w}), \lvert z\rvert < 2w$	$\frac{\sin^2 kw}{k^2 w^2} e^{ika}$	$\frac{k^4 w^4 - \sin^4 kw}{k^4 w^4 + \sin^4 kw - k^2 w^2 \sin^2 kw \cos ka}$

Analytical expressions soon get complicated for increasingly complex distributions. As Fourier transforms are rapid, a numerical evaluation of $\phi(k)$ is more feasible.

The paracrystalline lattice could be applied to *e.g.* lamellar systems. In Paper I it was used to model distribution between ionic layers in a sulfonated ionomer. It could also describe the arrangement of crystalline polymer separated by the amorphous polymer layers. Additionally one might allow the lamella to vary in thickness. Then there would be two distributions involved: One the lamella thickness and another one for their separation. In one approach, the scattering factor for the lamella is replaced by the average value $\langle F(k) \rangle$, which ignores the obvious correlation between lamella thickness and the separation. One could also adopt a different perspective and regard the system as a two phase structure with independent phase A and phase B layers. If the phases have constant density which changes in a stepwise fashion at the interface, one can assign scattering amplitudes $f_1 = i\delta/k$ and $f_2 = -i\delta/k$ to unit areas of the AB and BA interfaces respectively. Here $\delta = \rho_B - \rho_A$ is the density contrast which is neglected for now. This case is now analogous to a system of two types of particles (with opposite scattering factors in this case) arranged in a paracrystalline lattice with different distributions for the separation from 1 to 2 and from 2 to 1. Consequently, there are four partial correlation functions and four partial structure factors involved, but the total structure factor can easily worked out to be

$$S_1(k) = \frac{2}{k^2} \cdot \mathrm{Re}\frac{(1-\phi_1)(1-\phi_2)}{1-\phi_1\phi_2} \tag{48}$$

where ϕ_1 and ϕ_2 denote Fourier transformations of the two probability distributions. Again only gaussian and exponential distributions result in simple formulas. For two gaussians with $\sigma^2 = \sigma_1^2 + \sigma_2^2$

$$S_1(k) = \frac{2}{k^2} \frac{\sinh \frac{1}{2}\sigma^2 k^2 - \sinh \frac{1}{2}\sigma_1^2 k^2 \cos ka_2 - \sinh \frac{1}{2}\sigma_2^2 k^2 \cos ka_1}{\cosh \frac{1}{2}\sigma^2 k^2 - \cos kL} \tag{49}$$

[7] a denotes for lattice periodicity and z is small variation thereof

where $L = a_1 + a_2$ is the lamellar period. For two exponential distributions, with $c^2 = c_1^2 + c_2^2$

$$S_1(k) = \frac{2}{k^2} \frac{k^2c^2 + k^4c_1^2c_2^2 - k^2c_1^2(\cos ka_2 - kc_2 \sin ka_2) - k^2c_2^2(\cos ka_1 - kc_1 \sin ka_1)}{2 + 2(k^2c_1c_2 - 1)\cos kL + k^2c^2 + c_1^2c_2^2k^4 + 2(c_1 + c_2)k \sin kL} \tag{50}$$

One could also introduce correlations between adjacent nearest neighbor distances r. However, in this case one would have to calculate each $p_n(r)$ since the convolution form (44) is no longer valid. Such a calculation is difficult for any other distribution than gaussian [60]. For example, introduce correlation coefficient between adjacent neighbor-neighbor distances

$$t = \frac{\langle r_j r_{j-1} \rangle - \langle r_j \rangle \langle r_{j-1} \rangle}{\sigma^2} = \frac{\langle z_j z_{j-1} \rangle}{\sigma^2} \tag{51}$$

The correlation between n-nearest displacements z is then given by [60]

$$\frac{\langle z_j z_{j-n} \rangle}{\sigma^2} = t^n \tag{52}$$

Even though $p_n(r)$ can also be shown to be gaussian, this is of little use since the structure factor still has to be calculated numerically from (45). However, the authors of Ref. [60] considered a regular distorted lattice which is well worth looking into. Thus they had gaussian distribution for each displacement from the lattice position, z in our notation. What is said above about the correlation coefficients still holds. If σ_L denotes the variance for the displacement distribution, then for the nearest neighbor distance (r) and the n-nearest neighbors [60]

$$\sigma^2 = 2\sigma_L^2(1 - t)$$

$$\sigma_n^2 = 2\sigma_L^2(1 - t^n). \tag{53}$$

This still requires numerical calculation of the structure factor. The main result is that with a suitable choice of σ_L and t it produces short range paracrystalline distortions in a regular lattice which yet has long range order (LRO). Therefore it avoids the unlimited fluctuations which are inherent in the original paracrystal. Also, with superimposed Bragg reflection and diffuse paracrystalline peak it is much akin to systems which show quasi LRO encountered later in this introduction and could offer alternate model for these.

Surfactant micelles

Four papers in this thesis deal with substances called surfactants or amphiphiles used in conjunction with polymers. The remarkable properties of the surfactants have been studied for decades. As they are now becoming an important tool in tailoring new polymeric materials, it is instructive to first review some of this work. Most part of the underlying behavior may be well understood without considering the polymer.

The word amphiphile literally means loving both. 'Both' refers to oil and water which, as we well know, do not mix. The reason is their difference in polarity; water

molecules form a tetrahedrically coordinated network of hydrogen bonds and cannot incorporate the oil molecules unless large amounts of energy is brought to break some of these bonds. There is a negative mixing energy meaning that a molecule of oil[8] gains energy by associating with its own kind. This preference leads to macrophase separation. The dislike of the polar and nonpolar media is shown as a high surface tension between the separated phases. They try to create as little interface as possible to reduce the contact between the polar and nonpolar moieties.

An amphiphile is a special kind of molecule that has both hydrophobic and hydrophilic parts permanently attached by covalent bonds. The hydrophilic part is a polar end group and hydrophobic part consists of linear or branched hydrocarbon tail(s). Examples of amphiphiles[9] are fatty acids and their salts (soaps), phenols, sulfonates, ammonium salts or salts of phosphoric acids (phospholipids). Amphiphiles may also be classified as anionic, cationic or zwitterionic according to their charge[10]. Examples of amphiphiles occuring in this work are[11] PDP (phenol with an aliphatic tail), DBSA (benzene with sulfonic acid group and an alkyl tail), $Zn(DBS)_2$ (a zinc salt of previous), NaPal (Natrium Palmitate, sodium salt of an alkyl carboxyl acid), SDS (Sodium salt of an alkyl sulhponic acid) and AOT (sodium salt of a sulfonic acid which also forms two esters with branched monovalent alcohols).

The 'loving-both' disposition of an amphiphile makes it to seek to the oil-water interface. There it acts to reduce the surface tension, which moderates the growth of the phase regions to globally reduce the specific surface of the mixture. Because of this activity they are called *surfactants*. Aided by the surfactant, oil is capable of forming small droplets, *vesicles*, in the water. With sufficient amount of both present, these droplets may coalesce and both phases form interwoven channels, in which case the system forms a *microemulsion* and the surfactant is thus an *emulsifier*. Whenever the surfactants are referred to as lipids and this is mostly the case in biology, the corresponding structures that these form are *liposomes*. These phenomena are nothing modern. Humanity has used soaps and later detergents[12] for ages to make dirt (grease) soluble in water in tiny droplets. Thus the term *solubilizer*

[8] *Oil* is a common name for fats which are in the melt state at room temperature. Fat is an ester of glycerol with fatty acids which is the common name for long chained carboxylic acids. It is not important here that oils are esters, the key point is that they contain long hydrocarbon chains that are strongly hydrophobic (literally "water-fearing"). Similarly, polar molecules or groups that associate with water are said to be hydrophilic ("water-loving").

[9] The division of substances to hydrophobic and amphiphiles may appear confusing. For a molecule to be amphiphilic, a certain balance between hydrophilicity and hydrophobicity has to be realized. Thus aliphatic alcohols and amines are not amphiphiles though they have polar end groups. Not all fatty acids, salts or phenols are amphiphiles either, the chain has to have sufficient length, typically 8-18 carbon units. We can mentally arrange the molecules on a hydrophobicity axis with alkane chains at one end and water at the other. Amphiphiles would be found in between; some of them are soluble in water whereas others will only swell but may become soluble in different circumstances.

[10] For more terminology, a *soap* is an alkali salt of fatty acids. Fats etc. which are soluble in hydrocarbons and insoluble in water are commonly called *lipids*, which derives from the very word 'fat' from Greek. Phospholipids are important biological molecules. They are a formed of glycerol esterified with two fatty acids and one phosphoric acid. Usually the phosphoric acid (which is tribasic) is further esterified to a short alcohol. Acidic amphiphiles are anionic, those containing the amine group are cationic. *Zwitterions* contain both acidic and basic groups. Zwitterions are typically phospholipids esterified to alcohol amines such as choline.

[11] Their chemical names: PDP = pentadecyl phenol; DBSA = dodecyl benzene sulfonic acid; $Zn(DBS)_2$ = zinc dodecyl benzene sulphate; NaPal = sodium hexadecanoate; SDS = sodium dodecyl sulphate and AOT = Sodium 2-diethylhexylsulfosuccinate

[12] Detergents are cleaning agents made of anything else but natural fats. First synthetic detergents were alkylbenzenesulfonates, *i.e.* $Zn(DBS)_2$ is a detergent.

is also synonymous for a surfactant, though oil and water do not strictly speaking form a solution but are *micro-phase separated*. As an example of emulsion, a phospholipid called lecithin, which is found in egg yolk, makes oil and vinegar mix to form mayonnaise sauce.

Micellization

The above behavior is not in any way restricted to ternary systems involving water, oil and surfactant. Even pure amphiphiles tend to separate their polar and nonpolar parts. The relevant phenomena may be demonstrated in binary water/surfactant systems. In binary systems the droplets are referred to as *micelles* and the microemulsion specifically is known as the *sponge phase*. Most often the micelles are formed of the alkyl tails of the surfactants, but micelles of the polar component, *e.g.* *inverted micelles* also occur.

Whip together oil and water, they soon form larger and larger droplets until a complete macrophase separation has occurred. Similarly, if amphiphiles are mixed with water, dimers, trimers and multiplets start forming as the chemical potential experienced by the surfactant monomers decrease with increasing aggregate size. There exist a *critical micellar concentration* (CMC) above which all additional monomers go into micelles and micelles of infinite size appear spontaneously.

With binary amphiphile/water system, there is one distinction; every amphiphile molecule is at the surface of the multiplet. Without any free oil molecules present, the growth of the micelle is limited at least in one direction to the length of the alkyl tail. There is still repulsion between water and hydrophobic tails, which shows as a surface tension. This tension shrinks the surface and smoothens the corners as every tail is trying to get as far from the water as they possibly can. As is commonly known, the requirement of the least surface for a fixed volume leads to a sphere. This creates a barrier against micellar growth: Large micelles are energetically favorable, but in order to get there a micelle has to deform into a rod or a disc. *Infinite* cylinders or layers would be preferable[13], but for a *finite* micelle the potential barrier created by the rod ends or disc edges prevents micelle growth. On the other hand two micelles can not easily coalesce because there is generally a strong repulsive interaction due to hydration forces.

Thus micelles grow to a preferred size and shape which is governed by specific forces at the surface. Note, however, that a 'full-grown' micelle is by no means stable and rigid. Monomers are constantly hopping in and out with a time constant of a fraction of a second. The micelle itself is fluid with the monomers endlessly changing places and flip-flopping. It yields and deforms under external pressure and undulates due to thermal agitation. Thus the micellar solution (not really a solution but dispersion) is viscous, but fluid all the same. They are occasionally called *micellar fluids* or *complex fluids*.

Micellar form

As outlined, the hydrophobic interaction leads preferably to spherical form for small micelles (local minimum) whereas the lamellar form is the global minimum provided

[13] For equal smallest dimension (diameter equal to thickness D) the respective specific surfaces for lamellar, cylindrical and spherical forms are $2\phi/D$, $4\phi/D$ and $6\phi/D$ for , where ϕ is the surfactant volume fraction.

the lamellas are infinite[14]. Happily, there are other factors to affect the form of the micelles. For example, the hydrophilic groups may be placed in such a way to affect the molecular arrangement at the interface and therefore facilitate certain form for the micelle. The micellar form may be predicted by a number of different approaches.

Geometrical approach. Even simple notions about the dimensions of the amphiphilic molecule can give astoundingly accurate predictions [61]. The relevant parameters are the volume of the hydrophobic tail v, its length l and the surface area per amphiphile molecule a_0. The volume is more or less fixed whereas the length of the alkyl tail is less well defined. The end-to-end distance of the tail is somewhat less than its extended length. A long flexible chain coils more and temperature may affect its length significantly. Even so, there exists a well defined upper limit $l_c > l$ for the tail length [61].

The area of the amphiphile a_0 is determined by the headgroup as it connects to the polar medium [61]. Therefore it may be expected that this is another 'molecular' constant. Indeed, there is evidence that *e.g.* all soaps with different chain lengths fall to the same (small) relation of area/concentration curve [62]. However, the surface area may be controlled by changing the polar properties of the medium, *e.g.* by addition of salt ions or changing the pH [61]. With parameters v, l_c and a_0 set, the predicted order of phases is lamellar for $v < a_0 l_c < 2v$, cylindrical for $2v < a_0 l_c < 3v$ and spherical for $3v < a_0 l_c$.

Membrane theories. Membrane theories evaluate the free energy associated with the area and curvature of the interface. To improve on the previous theory, for example, note that the hydrocarbon tails are in a fluid state. They are in constant motion colliding with one another, which creates chain pressure. This tends to increase chain to chain separation and therefore induces outward curvature of the surface. Also, the hydrophilic groups tend to have a repulsive force between themselves, which works in opposite direction. The net effect is the preference towards a fixed curvature of the surface.

In membrane theories the molecular nature is abandoned and the energy is just written in terms of two invariants of the surface, the mean curvature H and Gaussian curvature K defined as

$$2H = \frac{1}{R_1} + \frac{1}{R_2}$$

$$K = \frac{1}{R_1 R_2} \tag{54}$$

where R_1 and R_2 are the two principal radii of curvature. These can be either positive or negative; a positive radius implies inward curvature. The free energy associated to the surface is [63]

$$F = \int \mathrm{d}S \left[\sigma + 2\kappa (H - H_0)^2 + \frac{1}{2}\bar{\kappa} K \right] \tag{55}$$

where σ is the surface tension, κ is the bending rigidity, $\bar{\kappa}$ is the saddle-splay modulus and H_0 is the spontaneous curvature of the surface. In the absence of both

[14] There are other forms of layered structures *e.g.* the sponge phase or the bicontinuous phases which are dealt with later on.

saddle-splay modulus and preferred curvature, the remaining parameters are σ and κ. General phase behavior may be outlined [64]. For large σ the system creates as little surface as possible forming small droplets or a sponge phase. For small (negative) σ normal smectic or nematic liquid crystal phases appear. The saddle-splay modulus $\bar{\kappa}$ affects the topology of the system. If $\bar{\kappa}$ is increased, at some point the system will undergo transformation to a phase with vanishing mean curvature everywhere and negative gaussian curvature. Such are the various bicontinuous cubic phases discussed later in the text.

For a ternary system, the form of the vesicles depending on the preferred curvature may be outlined [65]. This assumes fixed morphologies neglecting fluctuations. Let ϕ_o and ϕ denote volume fractions of oil and amphiphile. It is assumed that an amphiphile layer of thickness l_0 surrounds the regions of oil. If these regions are spherical we have $H = 1/R$ and $K = 1/R^2$. For cylindrical regions $H = 1/2R$ and $K = 0$ and for lamellar both are zero. Therefore

$$\frac{\phi}{\phi_o} \, (\equiv w H_0 l_0) = \begin{cases} 2l_0/R & \text{cylinders} \\ 3l_0/R & \text{spheres} \end{cases} , \tag{56}$$

where R is the radius and w is a dimensionless parameter related to the volume fraction. The free energy per unit area is then

$$f = 2\kappa H_0^2 \times \begin{cases} 1 & \text{lamella} \\ (w/4-1)^2 & \text{cylinders} \\ (w/3-1)^2 + \bar{\kappa} H_0^2 w^2/9 l_0^2 & \text{spheres} \end{cases} \tag{57}$$

giving phase sequence in terms of these microscopic parameters [66, page 144].

An interesting property might arise if the membrane (interface) has a particularly strong stiffness toward stretching but small bending rigidity. As one can easily demonstrate with a piece of paper, bending the membrane in one direction makes it stiffer in the other, since simultaneous bending modes would require stretching. If the membrane is flexible so that thermal fluctuations cause directional disorder in local scale, this does not imply that the membrane has disorder in the long scale, quite the contrary [67]. Now, long-scale bending would in this case produce directional anisotropy but nature resists this and chooses instead to moderate the bending so as to make the membrane flat at large length scales. Thus we have a case were local thermal undulations lead to long range order. This shows as the bending modulus being scale dependent.

Ginzburg-Landau models. In the Ginzburg-Landau approach the free energy is written as a functional expansion of an order parameter ϕ [66]

$$\mathcal{F}[\phi] = \int f(\phi, \nabla\phi, \nabla^2\phi) \mathrm{d}^3 r$$

$$f = c_1(\nabla\phi)^2 + c_2(\nabla^2\phi)^2 + \ldots + \sum_n a_n \phi^n \tag{58}$$

In binary systems, the order parameter is usually the density contrast $\phi = \rho_A - \rho_B$. Ginzburg-Landau theory is a phenomenological model, whose outcome is dictated by the choice of coefficients a_n and c_n. They predict micelle formation and the interface boundary profile and determine the behavior of the structure factor. Most

famous result is that given by Teubner and Strey [68] for microemulsion theory of strong amphiphiles. They chose for non-zero coefficients $a_2 > 0$, $c_1 < 0$ and $c_2 > 0$ which lead to structure factor

$$S^{-1}(k) \sim a_2 + c_1 k^2 + c_2 k^4. \tag{59}$$

This form of scattering factor is given by the Debye-Bueche correlation function [69]

$$g(r) = j_0(r/\ell) e^{-r/\xi} \tag{60}$$

where $j_0(x) = \sin x / x$ and the two characteristic lengths are

$$\left.\begin{matrix} \xi \\ \ell \end{matrix}\right\} = \left[\frac{1}{2} \left(\frac{a_2}{c_2} \right)^{1/2} \pm \frac{1}{4} \frac{c_1}{c_2} \right]^{-1/2}. \tag{61}$$

Stability requires $c_1^2 < 4 c_2 a_2$. Between $0 < c_1 < 2\sqrt{c_2 a_2}$ ordered domains exist but the structure factor peaks at zero wavevector length until $c_1 = 0$. This is called the *Lifshitz line*. For negative c_1 the peak shifts to non-zero wavevector and at $c_1 = -2\sqrt{c a_2}$ a transition to an ordered lamellar phase results. However, the above model also indicates unstability before the ordered phase sets in because the domain size would also diverge.

Mesoscopic phases of surfactants

As we have seen there is a preferred size and shape of the micelles. This is a big step toward ordered phases in surfactant systems, *i.e.* we may have translational instead of dilatational symmetry. The second requisite is forces between the micelles.

Forces between micelles

Intermicellar forces come in four categories: van der Waals, electrostatic, hydration and steric forces.

I) van der Waals interaction causes weak attraction between the micelles. Between two planar surfactant layers [61] the energy scales with layer separation d as d^{-2} but drops more rapidly as d^{-4} when the separation is much larger than the layer thickness. Similarly, for two spheres the vdW-energy scales as d^{-1} shifting to d^{-6} at large ($d \gg R$) separations. For two parallel cylinders the corresponding forms are $d^{-3/2}$ and d^{-5}.

II) Electrostatic interaction between the membranes results when the hydrophilic groups such as the carboxylate group (-COOH) become charged by proton dissociation or ion binding. It is usually repulsive and has exponential form $\sim e^{-\kappa d}$ where typical values for the decay length $1/\kappa$ are 3 Å per squareroot of (molar) electrolyte concentration. Electrostatic interactions are dominant over van der Waals forces whenever charges are involved.

III) Hydration forces. Near the interface, the polar matter (water) forms a frozen structure. This creates a steep potential barrier against the surfaces coming into contact. The extent of the resultant force is about 15 Å and may be described also with exponential decay.

IV) Steric forces have gained most interest in the recent years. Steric interaction arises from the motion of the fluid membranes (layers) as they collide with adjacent

membranes. This results in an outward pressure which acts to increase the membrane separation. The interaction energy f per unit area was derived by Helfrich [70]

$$f = 0.23k^2T^2/\kappa d^2, \tag{62}$$

where κ is the elastic modulus for a single membrane and d is the distance. Simulations suggest a smaller prefactor, 0.074 instead of 0.23, however [71].

The steric interaction competes with the van der Waals attraction, but should be dominant at large separation (of neighboring membranes) because of the faster decay of the latter.

If the repulsion is strong enough this is sufficient to induce ordering since in the ordered system the micelles are further apart. This distance is least in spherical form and biggest in lamellar which predicts a general phase sequence sphere→cylinder→lamelle with increasing interaction.

General remarks on the ordered phases

The formation of ordered phases depends on the amount of amphiphile and the amphiphile strength [66]. The strength is controlled in various ways depending on the amphiphile, *e.g.* by changing concentration or temperature. In ternary systems, a fluid phase is formed in equilibrium with water rich and oil rich phases. As the external field (temperature etc.) is varied, the concentration of oil and water in the middle phase[15] varies, and a sequence of ordered phases may be found. In binary systems, two phases, a water rich and amphiphile rich are formed. The latter is often found lyotropic.

The "classical" phase sequence with increasing amphiphile content is isotropic→cylinderical→lamellar. At the water rich side, these phases are inverted. Figure 5 gives a typical phase diagram of a fatty acid salt, which is one of the surfactants used in Paper II. Two curves meet the eye: the uppermost curve (T_I) separates the isotropic liquid from the lyotropic phases. The thick curve in the middle (T_C) separates the crystalline regions from liquid crystalline. The crystallization intercepts the phase sequence so no inverse phases are found in this case. All aliphatic hydrocarbons exhibit relative high crystallization temperatures depending on the number of unsaturated bonds. Branched chain surfactants such as AOT, form inverse-middle phase (inverse hexagonal with water cylinders) [72]. In potassium soaps, the region under crystallization curve may show two appearances [73]. One called *gel* is a translucent jelly and gives sharp diffraction peaks whose positions depend on the amount of water. The other *coagel* is opaque mass and gives diffraction peaks at the same position regardless of the amount of water. Thus gel phase has crystallized alkyl chains whereas the polar layer is in amorphous state and coagel is a dispersion of fully crystalline hydrated solid soap. Lithium and sodium soaps do not yield "gels". Potassium with even chain alkali carboxylate all form similar gels with interdigitated chains.

[15] It's called *middle phase* because being usually intermediate in density it appears physically in the middle of the test tube.

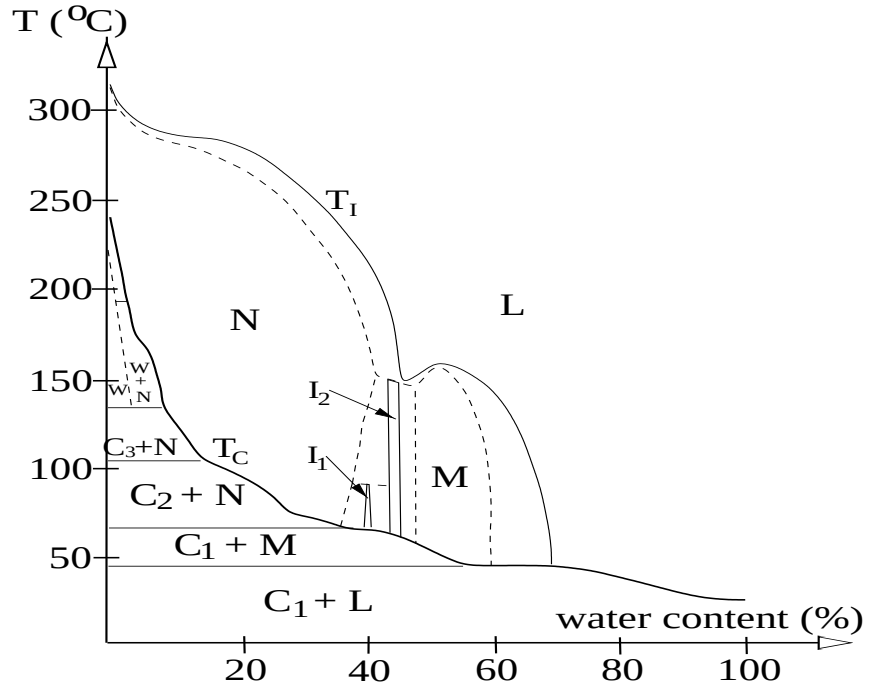

Figure 5: Simplified phase diagram of binary Sodium Dodecanoate / water system, after Madelmont et.al [75]. L=isotropic liquid (micellar solution), N=neat (lamellar), M=middle phase (cylindrical), C_1, C_2, C_3 are various crystalline phases, W=waxy, I_1, I_2 are intermediate mesomorphous phases. Apart from the waxy, pockets of several other forms appear along the temperature axis, which are not drawn. Intermediate to L, N, M, W and the I phases are regions of two phase coexistence.

The lamellar and cylindrical phases were first to be found[16]. They organize in *liquid crystalline* form which means that there's no periodicity other than that between the layers or cylinders. The isotropic phase is not actually structureless, but a disordered solution of spherical or cylindrical micelles.

In present view, the full sequence of phases is as depicted in Fig. 6. Ordered 3-D phases exist in two specific places in the phase diagram. Between the isotropic and hexagonal phases, *closed micelles* may form ordered structures, which have commonly cubic symmetry. More intriguing are the cubic phases which are found between lamellar and cylindrical structures, *i.e.* at positions I_1 and I_2 in Fig. 5 and V_1 and V_2 in Fig. 6. As their position suggests, they can hardly be based on closed micelles, but both water and amphiphiles form continuous structures. Thus the matter is said to be *bicontinuous*.

There was at first an understandable confusion between these two forms. In the early days it was commonly held that cubic phases consist of spherical micelles in some of the basic crystalline lattices such as the face centered cubic (fcc). Cubic and rectangular phases having 3-D symmetry were known to appear in high temperature phases found in *e.g.* fatty acid soaps [76, 77]. Then an alternative model was proposed by Luzzati and co-workers [78, 79] They reevaluated earlier results [80]

[16] In older literature 'neat' and 'middle phase' are synonymous to lamellar and cylindrical (hexagonal) forms [74].

and opined that most, perhaps all, space group determinations of fcc structures were incorrect. It was found that a variety of amphiphiles [81, 78, 79, 82, 83] showed strikingly similar structure, which by x-ray scattering seemed to agree with a network of connected rods. The space group was determined as 230 ($Ia\bar{3}d$) and the position of the rods implied the existence of two unconnected networks of rodlike water channels in hydrocarbon matrix.

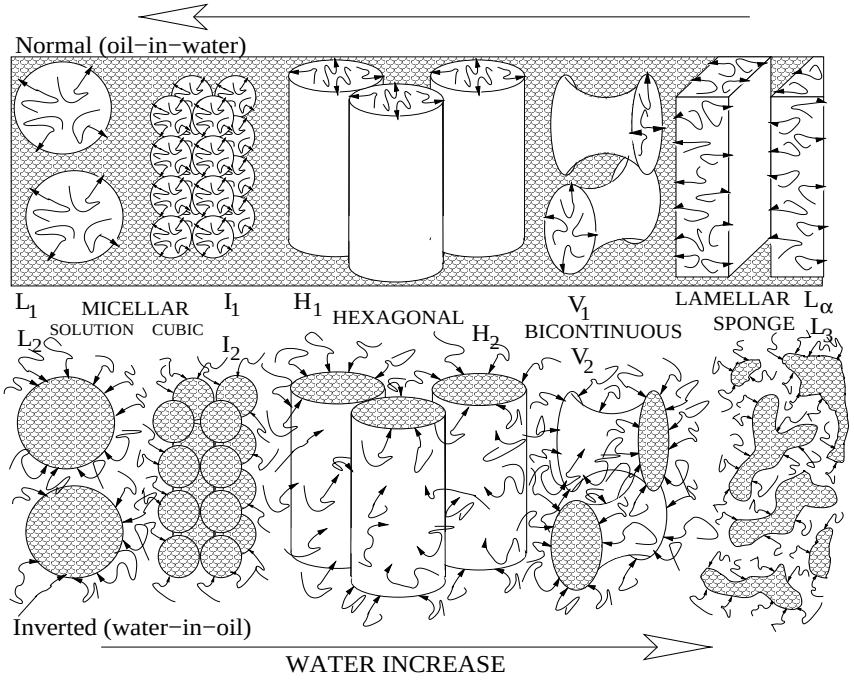

Figure 6: General order of phases found in surfactant/water systems and their standard symbols. Not all phases necessarily appear and there are regions where two phases may be found in coexistence.

Scriven [84] made an important contribution concerning the nature of these phases. Though he claims that bicontinuous structures in fluids have never been contemplated before in spite of Luzzati's and others' work presented in the same journal a few years earlier, he was the first to draw attention to the role of the surface partitioning the two phases, which he assumed as *infinitely periodic minimal surfaces* (IPMSs). Thus the hydrocarbon matrix is really a surfactant bilayer which divides the two water networks into two symmetric subvolumes. The center of this bilayer is at the IPMS. The number of different IPMSs is stated to be 17 [85]. However, it is now widely believed that just three of these appear in practice. These are Schwartz's P-surface, Schwartz's D-surface and Schoen's G-surface[17]. Figure 12 gives an illustration of these.

The first observed phase $Ia\bar{3}d$ is based on the G-surface [76] and it has also proved to be the most common. Numerous examples may be found in the review articles of cubic surfactant [86] and membrane lipids [87]. Reports of the two other surfaces are still rare to date, though researchers have been savvy to look for these.

[17] "P" is for primitive, "D" for diamond and "G" for gyroid

The D-surface was found in Glycerol monooleate (GMO) [88]. It forms a primitive cubic structure with a tetrahedral space group 224 ($Pn\bar{3}m$). The P-surface seems rarest of the three and it's existence has even been debated [89]. The GMO was at first determined as based on Schwartz's P-surface with space group 221 ($Pm\bar{3}m$) [90] or 229 ($Im\bar{3}m$) [91], but was later corrected to be based on the D-surface. A recent article [92] reports the space group $Im\bar{3}m$ in a surfactant referred to as $C_{17}E_{84}$ but in this case the aggregates are said to be of closed spherical form, according to NMR. Gruner [93] reports this type of structure in methylated DOPE (dioleoylphosphatidylethanolamine) which shows signs of superimposed $Pn\bar{3}m$ (D-surface) and $Im\bar{3}m$ (P-surface or spherical bcc) structures. Recently, Templer has reported seen all three IPMS's in mixtures of phospholipides and fatty acids [94, 95], while Jones et al. [96] have investigated ternary water/toluene/DDAB which is said to organize in this morphology[18].

In addition, there are a few occationally appearing phases whose form has been controversial. The first was found not long after the observation of $Ia\bar{3}d$ [98] in an analogous system [99]. The space group was determined as 223 ($Pm\bar{3}n$). The structure was suggested to be partly connected, consisting of both rodlike network and quasi-spherical micelles. Inspired by this, Luzzati and coworkers subsequently proposed similar 'hybrid' phases derived from the bicontinuous phases by replacing one network with closed micelles [100]. Thus from the G-surface one derives space group 212 ($P4_332$) and from the D-surface a space group 227 ($Fd\bar{3}m$) is obtained.

The partly connected structure has been rejected by Eriksson and other workers in the field. Based on surfactant self-diffusion results, the $Pm\bar{3}n$ structure is shown to be formed of closed micelles [101]. A plausible model is due to Fontell [102], and is effectively the same as solid O_2 and N_2, with short rod-like micelles replacing the diatomic units. Also the proposed 'hybrid' $Fd\bar{3}m$ form have later been reevaluated [103] in favor of closed micelles [104]. It is possible that the two forms other than $Pm\bar{3}n$ (*i.e.* 212 and 227) result from impurities in form of coexisting phases. The $Pm\bar{3}n$ form is frequently encountered, however, *e.g.* in the CS/sodium palmitate/water system studied in Paper II. It has been suggested that all the phases in in the *micellar cubic* position (I_1) have this structure ($Pm\bar{3}n$) [86]. At the water rich side (I_2), the tendency to form organized phases seems to be lower [86] and until recently no cubic phases had been identified. It now appears that the micellar ($Fd\bar{3}m$) phase is the dominant form in this position [105, 103]

Lamellar morphology

The lamellar phase is a one dimensional crystal with the single lattice vector perpendicular to the lamellae. One can distinguish two order parameters; translational and orientational order. Even though they are one dimensional periodic structures, the lamellar phases cannot often be described with the paracrystalline model. To see where the distinction arises, let us consider the lamellar phase in the membrane approach, *e.g.* where surfactant bilayers are separated by polar media. Recalling what was said about the effect of thermal fluctuations, in the extreme cases the system may show quite remarkable division to long range order (LRO) and short

[18] These authors place the P-surface in $Pn\bar{3}m$ space group [97]. There are more than one space groups which give the same structure. However, as this space group is also used for the D-surface, the normal assignment is used here, *i.e.* $Ia\bar{3}d$ for G, $Pm\bar{3}n$ for D and $Im\bar{3}m$ for P.

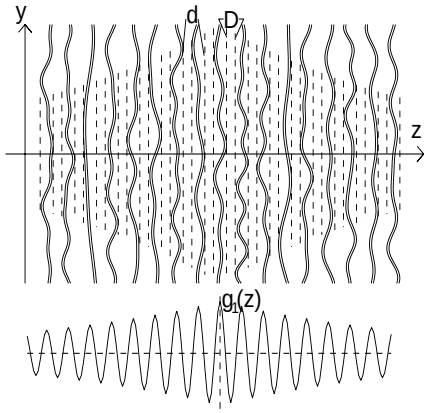

Figure 7: Schematic figure showing undulating lamellae in confined space.

range disorder. This is schematized in Fig. 7. Thus very flexible membranes, when little elastic energy is associated with the bending modes, may be forced to periodic lattice positions so as to allow ample space for oscillations of each individual membrane. As we have learned, the order is never strictly periodic but may nevertheless show *quasi-long range order*. The dynamics of each membrane is equivalent to as if it were confined between two rigid walls of width $2(d-D)$ where d is the average lattice period and D is the closest distance between the membranes due *e.g.* to hydration forces and the thickness of the membrane.

The disorder at short range is shown by the broad maxima in the correlation function $g_1(z)$ (drawn sinusoidal in Fig. 7) in place of sharp delta functions. One cause of this is that the higher order reflections in the diffraction pattern can be quite weak. It is common that the higher orders are minor to the first order by a factor 10^{-4}. The actual distribution of the density along the lattice period d (structure factor of the membrane) has the same effect. The density profile depends on the strength of phase segregation and for weak segregation it is also sinusoidal. In this case the 'membranes' are replaced by surfaces of constant density.

The quasi-LRO means that the correlation function is ultimately damped to zero at large membrane-membrane distances. The damping function is observed in the profile of diffraction peak. For example, an exponential decay of the correlation function leads to lorenzian shaped profile of the Bragg reflection. In practice the decay is slower [106, 107] and can be related to the elastic properties of the membrane and the intermediate matter. Consider the undulations of the n:th lamella as local displacements $u_n(y)$ in the z-direction from its equilibrium (lattice) position. The undulations are associated to an elastic wave denoted by wave vector $\mathbf{q} = (\mathbf{q}_y, q_z)$ where the z-axis is chosen perpendicular to the lamellae (*c.f.* Fig. 7) and $\mathbf{q}_y$ is in the plane of the lamellae.

The waves propagating along the z-axis will just compress the matter leaving the membranes flat, whereas waves along the the plane of the lamellae do not change the distance between the membranes and produce only bending of the membranes. The energy associated with the compression is $\frac{1}{2}Bq_z^2u^2$, where B is compressibility. The bending energy (*c.f.* Eq.55) depends on membrane rigidity κ and curvature. For a sinusoidal wave, the curvature is $R^{-1} \sim q_y^2 u$ and the energy is $\frac{1}{2}\kappa q_y^4 u^2$.

The sum of these two[19] terms is subject to energy equipartition; each wave $\mathbf{q}$ carries energy kT and therefore the square amplitude is moderated by the sum. Then the fluctuation is given by

$$\langle u^2 \rangle = \frac{kT}{4\pi^3} \int_{\pi/L_z}^{\pi/d} \mathrm{d}q_z \int_0^\infty \frac{2\pi q_y \mathrm{d}q_y}{Bq_z^2 + \kappa q_y^4}. \tag{63}$$

[19] Additional energy terms might include external magnetic field $\mathcal{H}$, to align the membrane normals to the z-direction, and thus to the transverse (y) component would be added $\frac{1}{2}\chi\mathcal{H}^2 q_y^2 u^2$ where χ is the magnetic susceptibility.

The cut-off frequencies are given by membrane separation d and the thickness of the lamellar stack L_z. We consider here infinite homogeneous lamella so that the limits of the inner integral can be taken from zero to infinity. One obtains [106]

$$\langle u^2 \rangle = \frac{kT}{8\pi(\kappa B)^{1/2}} \ln L_z/d. \tag{64}$$

This restates Landau's argument that in infinite one dimensional system, the fluctuations also grow infinite and perfect lamellar crystals cannot exist [56, pp. 432-6]. The ratio of parameters κ and B defines whether the fluctuations are in the transverse or longitudial direction of which the latter is the only one disrupting order. Thus the quantity $(\kappa/B)^{1/2} \equiv \lambda$ determines the decay of undulations.

The correlation between displacements is given by

$$\langle |u_n(\mathbf{y}) - u_0(0)|^2 \rangle = \frac{kT}{2\pi^3 B} \int \mathrm{d}q_z \int \mathrm{d}\mathbf{q}_y \frac{1 - \cos(\mathbf{y} \cdot \mathbf{q}_\mathbf{y} + \frac{2\pi n}{d} q_z)}{q_z^2 + \lambda^2 q_y^4}. \tag{65}$$

For large n it has asymptotic solution [107]

$$\simeq \frac{kT}{4\pi(\kappa B)^{1/2}} \left[2 \ln \frac{\gamma y}{2a} + E_1(\frac{y^2 d}{8\pi n \lambda}) - f(\frac{\lambda d}{\pi a^2}) \right], \tag{66}$$

where $\ln \gamma = 0.577\ldots$ is the Euler constant, and functions E_1 and f are defined by

$$E_1(x) = \int_x^\infty \mathrm{d}t \frac{e^{-t}}{t} = -\ln \gamma x - \sum_{n=1}^{\infty} \frac{(-x)^n}{n \cdot n!}$$

$$f(x) = \frac{2}{\pi} \int_0^x \mathrm{d}t \frac{\arctan t}{t}. \tag{67}$$

In the normal direction $\mathbf{y} = 0$ in particular, Eq.(65) yields

$$\langle |u_n - u_0|^2 \rangle = \frac{kT}{4\pi(\kappa B)^{1/2}} \left(\ln \pi n + \ln \gamma - \mathrm{ci}\ \pi n \right), \tag{68}$$

where the cosine integral (ci) is an insignificant contribution. The logarithmic decay creates a singularity centered at the position of the Bragg peaks $\mathbf{k}_n = 2\pi n \hat{\mathbf{z}}/d$. For scattering vectors close to these peaks, *e.g.* $\mathbf{K} = \mathbf{k} - \mathbf{k}_m$, the scattering intensity is predicted to follow

$$I \sim K_z^{-2+\eta} K_y^{-4+2\eta} \tag{69}$$

where the deviation from the "regular" lorenzian shape is dependent on the parameter

$$\eta = \frac{kT k_n^2}{8\pi(\kappa B)^{1/2}}. \tag{70}$$

The dependence on the order of the reflection, $\eta \sim n^2$, is essentially created in making a harmonic approximation for the displacement correlation function [108, 107]

$$g(y,z) = \exp\left(-\frac{1}{2} k_z^2 \langle |u_n(y) - u_0(0)|^2 \rangle \right). \tag{71}$$

For the present case

$$g(y,z) = \left(\frac{2d}{y}\right)^{2\eta} \exp\left(-\eta\left[2\ln\gamma - f(\frac{\lambda d}{\pi a^2}) + E_1(\frac{y^2}{4\lambda z})\right]\right). \tag{72}$$

The dependence on n has also been verified in experiment [109]. If the repulsion is due to membrane fluctuation, *i.e.* the Helfrich interaction [70], the theory predicts for the first order reflection[20]

$$\eta_1 = 1.33(1 - D/d)^2. \tag{74}$$

This was demonstrated to hold in the same paper [109].

The profile of the m:th Bragg reflection may be obtained from

$$I(k) \sim \int \mathrm{d}z \int g(y,z) e^{-\pi r^2/L^2} \frac{e^{izk_m} \sin kr}{kr} \mathrm{d}^2 y \tag{75}$$

with $r^2 = z^2 + y^2$ and $k_m = 2\pi m/d$. The gaussian term $e^{-\pi r^2/L^2}$ takes into account the finite size of the crystalline regions. Another way is to calculate the one dimensional structure factor similar to a paracrystalline stack of N layers [110]

$$S_1(k) = 1 + 2\sum_{n=1}^{N-1}\left(1 - \frac{n}{N}\right) \exp\left(-\frac{k^2 d^2 \alpha_n + n^2\delta^2 d^2/2}{1 + 2\delta^2 d^2 \alpha_n}\right)$$

$$\times \cos\left(\frac{ndk}{1 + 2\delta^2 d^2 \alpha_n}\right) / (1 + 2\delta^2 d^2 \alpha_n)^{1/2}, \tag{76}$$

with α_n from Eq.(68)

$$\alpha_n = \frac{\eta}{4\pi^2}\left(\ln \pi n + \ln \gamma\right) \tag{77}$$

A gaussian instrumental resolution δ is directly implemented in Eq.(76). Structure factors given by the equation are portrayed in Fig. 8. With vanishingly small η, all orders of the Bragg reflections are equally intense and their width is defined by the thickness of the stack of lamellas. As η is increased, the higher order peaks are rapidly damped and the diffuse tail of each peak becomes conversely larger, as predicted. The one di-

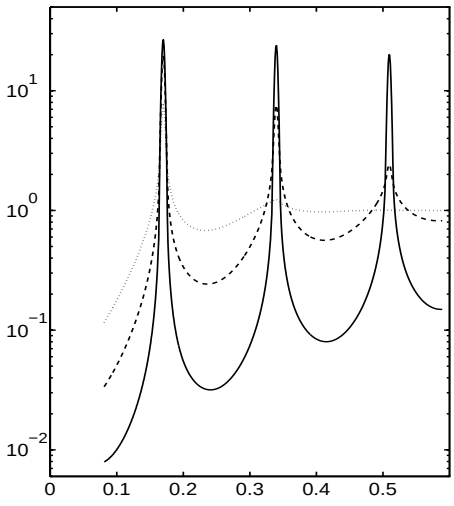

Figure 8: One dimensional structure function $S_1(k)$ for a stack of 60 lamella and $\eta = 0.01$ (solid curve), $\eta = 0.1$ (dashed curve) and $\eta = 0.4$ (dotted curve)

[20] This dependence is obtained by equating the spring constant (compressibility) B with the second derivative of the interaction energy (62) with the membrane separation written as $d - D$

$$B = 1.38k^2T^2/\kappa(d - D)^4. \tag{73}$$

mensional intensity needs to be multiplied with the scattering factor and averaged over different orientations (powder averaging) before comparison with experiment is made.

An example of experimental data is presented in Fig. 9. The data is from a system of AOT/water/polymer, measured with the point focusing setup in HU for three hours. AOT[21] is frequently studied surfactant [111, 112, 113]. It is a branched chain surfactant and does not crystallize readily. Pure AOT organizes in inverse hexagonal form [111] and can dissolve up to 16 % of water in this structure. For increasing water content, the normal phase sequence $H_1 \rightarrow V_1 \rightarrow L_\alpha$ is found. At the lamellar phase the structure is simply *swelled* by the water. The thickness of the AOT bilayer remains constant at 19-21 Å [113] while water pushes the bilayers apart in linear relation to the volume fraction. In Fig. 9 the lamella separation is 76 Å.

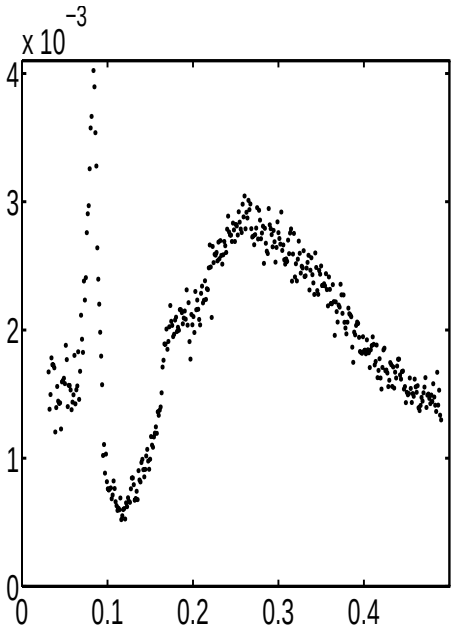

Figure 9: Experimental intensity curve for AOT/water/DMAA system for 25/65/10 % composition

Up to 82 % of water can be incorporated while the structure still keeps in the well ordered lamellar state. This is by no means unusual. Very flexible membranes can show extreme swelling and LRO even as little as 0.5 % of the surfactant present and produce 6500 Å lattice spacing [114, 109]. This type of behavior is observed in neutral lipids with sufficiently small bending modulus $\kappa \sim kT$ in which case steric effects dominate over the van der Waals interaction. In charged lamellar system, the longer ranged electrostatic interaction supersedes steric repulsion due to undulations and the lamellas flatten [115].

Cylindrical morphology

Cylindrical micelles form a two dimensional analogue of close-packing, which is the hexagonal lattice. The hexagonal lattice is span by two vectors **a** and **b** at 120° angles, and both of length a. In perfect crystals, cylinders occupy the lattice positions denoted by Miller indices (n, m) at $\mathbf{R}_{nm} = n\mathbf{a} + m\mathbf{b}$. However, as was the case in previous section, perfect crystals do not exist in two dimensions neither. Thus we

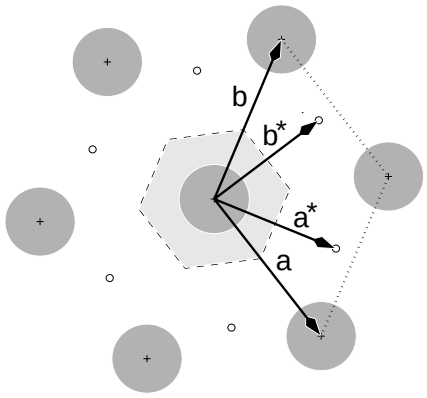

Figure 10: Definition of a hexagonal lattice.

[21] See page 22 for its description; D^a Isabel Esteban Ipacios of UNED, Spain is kindly acknowledged for providing me this sample

expect fluctuations to diverge with system size here also. Let us consider again integral (65) where the bending energy now refers to that of the cylinders. Now the equation is written as

$$\langle |u_{nm}(z) - u_{00}(0)|^2 \rangle = \frac{kT}{2\pi^3 B} \int \mathrm{d}q_z \int \mathrm{d}\mathbf{q}_y \frac{1 - \cos(\mathbf{R}_{nm} \cdot \mathbf{q}_y + z q_z)}{q_y^2 + \lambda^2 q_z^4}. \tag{78}$$

The z-direction is now taken along the cylinder axis. For $z = 0$,

$$\langle |u_{nm} - u_{00}|^2 \rangle = \frac{kT}{4\sqrt{2}\pi^2 B^{1/2} (\kappa B)^{1/4}} \int^{\text{1st B.z.}} \mathrm{d}\mathbf{q}_y \frac{1 - \cos(y q_y)}{q_y^{3/2}}, \tag{79}$$

where the integral is over the first Brillouin zone of the lattice, the gray hexagon in Fig. 10. Thus

$$\int \mathrm{d}\mathbf{q}_y \frac{1 - \cos(y q_y)}{q_y^{3/2}} = \sqrt{\frac{\pi}{a}} \int_0^1 \mathrm{d}x \int_0^1 \mathrm{d}y \frac{3 - \cos(f) - \cos(f - 2\pi n x) - \cos(f - 2\pi m y)}{(x^2 + y^2 - xy)^{3/4}} \tag{80}$$

where

$$f = \frac{4\pi}{3}(nx + my - ny/2 - mx/2).$$

Numeric solution suggests that the integral will depend only on the distance $R_{nm}/a = r = (n^2 + m^2 - nm)^{1/2}$ and has an extremely slow double logarithmic divergence,

$$\simeq \sqrt{\frac{\pi}{a}} \left[\frac{13}{2} \ln(\ln r + \sqrt{2}) + 4 \right] r^{-0.039}. \tag{81}$$

This places the hexagonal phase somewhere between lamellar and solid. The diffuse scattering is expected to be weaker than for the lamellar case.

For a more elaborate derivation, the interaction between the cylinders is to be included. This is accomplished by introducing, in addition to the bending energy, a free energy cost for the fluctuations of the cylinder axis direction from the local average (the nematic field) [116]. Two new parameters called the Frank constants, κ_1 and κ_2, for splay and twist deformations are introduced. Also, for proper calculation of the elastic energy, the displacements and the single elastic constant B, are replaced with the strain tensor and the so called Lamé's coefficients λ and μ. The free energy is then [117]

$$F_q = \frac{1}{2} \left[(\lambda + 2\mu) q_y^2 + \kappa_1 q_y^2 q_z^2 + \kappa_3 q_z^4 \right] u_L^2 + \frac{1}{2} \left[\mu q_y^2 + \kappa_2 q_y^2 q_z^2 + \kappa_3 q_z^4 \right] u_T^2 \tag{82}$$

in which the displacement is separated to longitudial and transverse parts u_L and u_T and κ_3 is the bending coefficient previously written without a subscript. The correlation integral is now

$\langle |u_{nm} - u_{00}|^2 \rangle =$

$$\frac{kT}{4\pi^3} \int \mathrm{d}q_z \int \left[\frac{1 - \cos(\mathbf{R}_{nm} \cdot \mathbf{q}_y)}{(\lambda + 2\mu) q_y^2 + \kappa_1 q_y^2 q_z^2 + \kappa_3 q_z^4} + \frac{1 - \cos(\mathbf{R}_{nm} \cdot \mathbf{q}_y)}{\mu q_y^2 + \kappa_2 q_y^2 q_z^2 + \kappa_3 q_z^4} \right] \mathrm{d}\mathbf{q}_y. \tag{83}$$

As we expect again the result to depend only on $R_{nm} = ra$, it should also be permissible to change the integral over a sphere, whose area matches that of the Brillouin zone, $\pi q_0^2 = 8\pi^2/\sqrt{3}a^2$. Then the integral is transformed to one dimensional with the expense of having to evaluate the Bessel function J_0

$$\langle |u_r - u_0|^2 \rangle = \frac{kT}{\eta_1} \int_0^1 \frac{1 - J_0(crx)}{(x^2 + \gamma_1 x)^{1/2}} \mathrm{d}x + \frac{kT}{\eta_2} \int_0^1 \frac{1 - J_0(crx)}{(x^2 + \gamma_2 x)^{1/2}} \mathrm{d}x \qquad (84)$$

where

$$\begin{aligned} c &= 8^{1/2}\pi^{1/2}/3^{1/4} \approx 3.8093, \\ \eta_1 &= 4\pi\kappa_1^{1/2}(\lambda + 2\mu)^{1/2}, \\ \eta_2 &= 4\pi\kappa_2^{1/2}\mu^{1/2}, \\ \gamma_1 &= 2\kappa_3^{1/2}(\lambda + 2\mu)^{1/2} a/\kappa_1 c, \\ \gamma_2 &= 2\kappa_3^{1/2}\mu^{1/2} a/\kappa_2 c. \end{aligned}$$

For appreciable γ_1 or γ_2, the integrals will diverge slowly (with the double logarithmic form as previously) whereas for vanishing these terms, the divergence will be 'only' logarithmic.

The scattering of a finite hexagonal crystal might then be evaluated from the two dimensional analog[22] of Eq.(76)

$$S_2(k) = 1 + \sum_{r<D} G_D(r) P_r \exp\left(-k^2 \langle |u_r - u_0|^2 \rangle\right) J_0(kr), \qquad (85)$$

where $G_D(r)$ is the autocorrelation function of a circle of diameter D

$$G_D(r) = \frac{2}{\pi}\left[\arccos\frac{r}{D} - \frac{r}{D}\sqrt{1 - \frac{r^2}{D^2}}\right], \qquad (86)$$

and P_r is the number of lattice points at distance r from an arbitrary lattice point in an infinite lattice.

The structure factors in Fig. 11 are calculated using the double-logarithmic dependence (81). The parameters are chosen so that the η value for closest neighbors corresponds to same values in the lamellar case. The diffuse scattering increases rapidly with increasing η as in the lamellar case as this is mostly due to closest point correlation. Note the skewed form of the first peak at large η. Due to the slow divergence, Bragg peaks are now more pronounced.

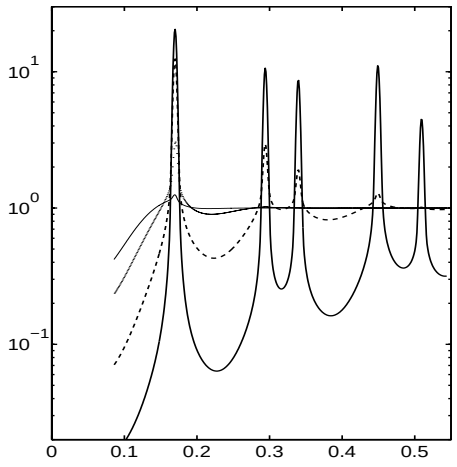

Figure 11: Two dimensional structure function $S_2(k)$ for a bundle of 60 unit cells in diameter and $\eta = 0.01$ (solid curve) , $\eta = 0.1$ (dashed curve) , $\eta = 0.4$ (dotted curve) and $\eta = 0.8$ (thin solid curve).

[22] The powder averaging in this case means division by k instead of k^2 as was the case in one dimension

Unlike the lamellar system, the hexagonal phase cannot support dilution. In the ordered structures the cylinders are tightly packed with $a/D \leq 1.2$. For a higher ratio the system is weakly ordered and is viewed as a nematic liquid. Structure factors for these have been derived within RPA. The solution is formally similar to Eq.(38), but orientation correlations (nematic interaction) are taken into account and therefore the linear response theorem is applied in the position-orientation space. The structure factor is of form [118]

$$S(k) = \frac{P_0(k) + R_0(k)}{1 + v\,(P_0(k) + R_0(k))}, \tag{87}$$

where P_0 is the form factor of the cylinders and R_0 contains the effect of orientation. The result describes not only cylindrical rods, but stiff polymer chains as well. The functions can be represented by integrals along the chains [118]

$$P_0(\mathbf{k}) = \frac{n}{L}\int_L \mathrm{d}\mathbf{r}\int_L \mathrm{d}\mathbf{r}'\langle e^{i\mathbf{k}\cdot(\mathbf{r}-\mathbf{r}')}\rangle \tag{88}$$

$$U_0(\mathbf{k}) = \frac{3}{2}\frac{n}{L}\int_L \mathrm{d}\mathbf{r}\int_L \mathrm{d}\mathbf{r}'\langle e^{i\mathbf{k}\cdot(\mathbf{r}-\mathbf{r}')}\left[(\mathbf{u}\cdot\hat{\mathbf{k}})^2 - \frac{1}{3}\right]\rangle$$

$$T_0(\mathbf{k}) = \frac{3}{2}\frac{n}{L}\int_L \mathrm{d}\mathbf{r}\int_L \mathrm{d}\mathbf{r}'\langle e^{i\mathbf{k}\cdot(\mathbf{r}-\mathbf{r}')}\left[(\mathbf{u}\cdot\hat{\mathbf{k}})^2 - \frac{1}{3}\right]\left[(\mathbf{u}'\cdot\hat{\mathbf{k}})^2 - \frac{1}{3}\right]\rangle,$$

where $\mathbf{u}$ is the local tangent of the chain, n is polymer density and functions U_0 and T_0 define R_0 by

$$R_0(k) = \frac{2v_1U_0^2(k)}{3\,[1 - v_1T_0(k)]}, \tag{89}$$

where v_1 represents the strength of nematic interaction.

Schoot et al. have used a different method of calculation of the structure factor from the same premise [119]. In their formulation the structure factor is derived for rodlike molecules (cylinders) of diameter D and length L

$$S(k) = \frac{F^2(k)}{F(k) + \frac{\pi}{4}L^2Dn\left(2F^2(k) + \frac{5}{4}G^2(k)\right)}, \tag{90}$$

where $F(k)$ is the form factor of the rods [120], (same as P_0 in Eq.(88))

$$F(k) = \frac{2}{kL}\int_0^{kL}\frac{\sin t}{t}\mathrm{d}t - \left(\frac{\sin kL/2}{kL/2}\right)^2 \tag{91}$$

and

$$G(k) = \frac{3}{k^2L^2}\left(1 - \frac{\sin kL}{kL}\right) - \frac{1}{2}F(k).$$

Bicontinuous phases

After their discovery, the bicontinuous cubic phases have attained considerable attention among the ordered phases. These structures may be described in two basic ways; one is the Luzzatti's network of connected rods, the second is the minimal surface approach. For visualization, the rod model is definitely better.

Imagine identical volumes, blocks, having n arms (rods) which connect to n neighboring blocks. Simplest of such blocks, capable of forming a periodic three dimensional structure, would then have have $n = 3, 4$ or 6. The structure is then said to be connected 'three-by-three', 'four-by-four', or 'six-by-six'. The arms are expected to be coplanar in the first case, tetrahedrally oriented in the second case and orthogonal in the final case. The question now arises, how the blocks look like, after their surface is minimized while maintaining their volume and connectivity.

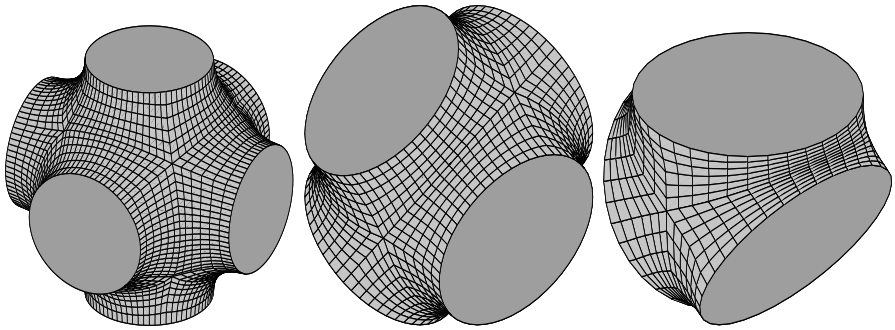

Figure 12: Surface-minimized 6-armed, 4-armed and 3-armed volume blocks.

Finding such a surface exactly is a tedious task, but for the present purposes we make a coarse calculation, representing the asymmetric surface element by its 3 by 3 lowest Fourier components. In Fig. 12 are resulting surfaces for the three cases for arbitrarily chosen volumes. When (and if) these can be joined to form an infinite network, this network will be the one with least surface for a given volume fraction of the blocks.

The surfaces in Fig. 12 are the prototypes of the P,D and G surfaces. Strictly, they are not yet *minimal surfaces*, for a minimal surface divides the space in two identical subvolumes. To locate the minimal surface, consider the behavior of the area as a function of volume as given in Fig. 13. The distance between the blocks in each case is scaled to unity. It is noted that for volume greater than 0.28, the periodic surfaces contain less area than the sphere. More importantly, the curves have maxima at volumes $1/2$, $4/3\sqrt{3}$ and $\sqrt{2}$ and they are symmetric about this point. The reason is obvi-

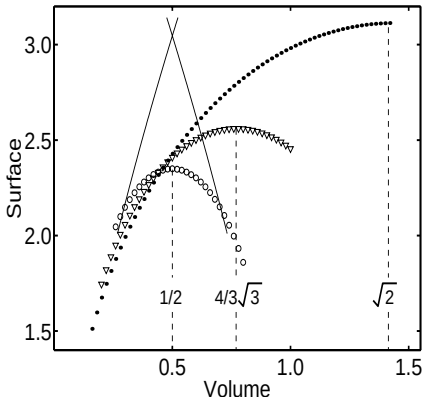

Figure 13: Surface areas for the 3-armed (•), 4-armed (▽) and 6-armed (○) blocks. Surface area for a sphere (sc) is shown for comparison.

ous: The network formed by these blocks also defines a connected subvolume of the 'outside', the surface of which is minimized concurrently. Though this does not prove that this second volume is identical, Fig. 13 suggests that such may be found. The position of the maxima then correspond to a point where both volumes are identical. These are the minimal surfaces.

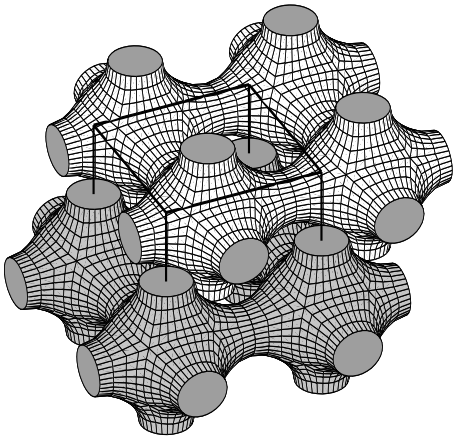

Figure 14: Two intertwining networks formed by the 6-armed blocks.

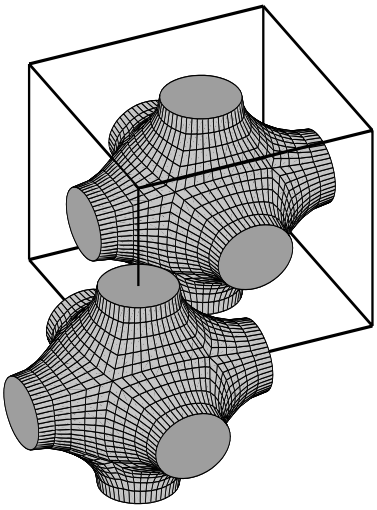

Figure 15: Unit cell of systems based on the P surface.

For the P and D surfaces, these networks are easily found because they constitute the most obvious ways of connecting the 6-arm and 4-arm blocks. Fig. 14 shows that if the 6-armed blocks occupy and connect the corners of a simple cubic (sc) lattice, the second subvolume is at the body centered positions and has the same symmetry. The unit cell contains two blocks as presented in Fig. 15 and the space group is the body centered $Im\bar{3}m$. When both volumes fill half the space, two surfaces coalesce into a single IPMS. It's area is 2.345 per unit volume as given directly by the maximum of Fig. 13.

Likewise, the 4-armed blocks are connected to form a diamond network. It is a more head-ache producing exercise to ascertain that another subvolume with the same symmetry appears translated half the unit vector of the conventional unit cell (fcc for diamond), which then contains 16 of our basic blocks (*c.f.* Fig. 16). Due to the translation the unit cell reduces to the simple cubic $Pn\bar{3}m$ with 1/8 th of the original cell size and two blocks per unit cell (Fig. 17).

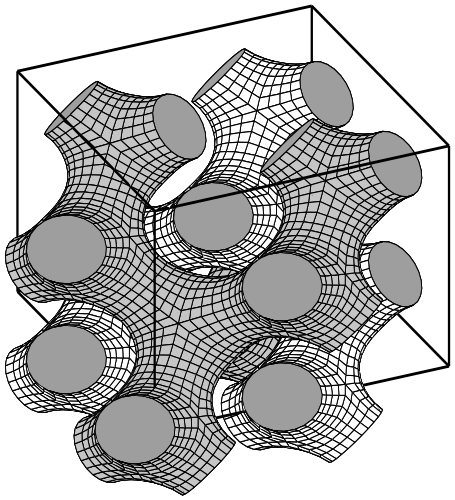

Figure 16: Two intertwining networks formed by the 4-armed blocks.

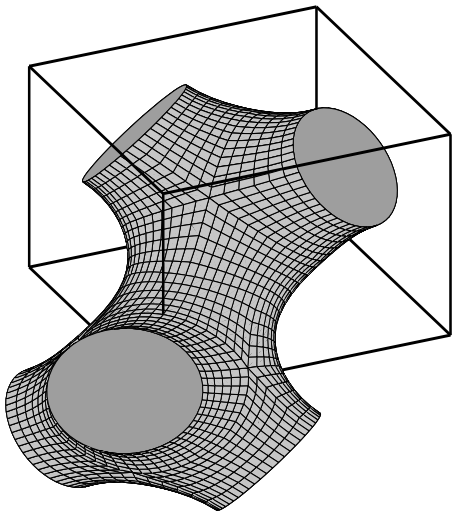

Figure 17: Unit cell of systems based on the D surface.

In the case of three coplanar arms, the most obvious choice would be to construct planar hexagonal networks as in graphite. This does not fill space completely, as is demonstrated in Fig. 18. However these (the vertical networks in Fig. 18) make structures known as *hexagonally perforated layers* (denoted R_{II}) which are known in polyelectrolytes and block-copolymer systems. Such networks are also suggested to exist in high temperature phases in anhydrous soaps and *e.g.* lecithin with small fraction of water [82, 83].

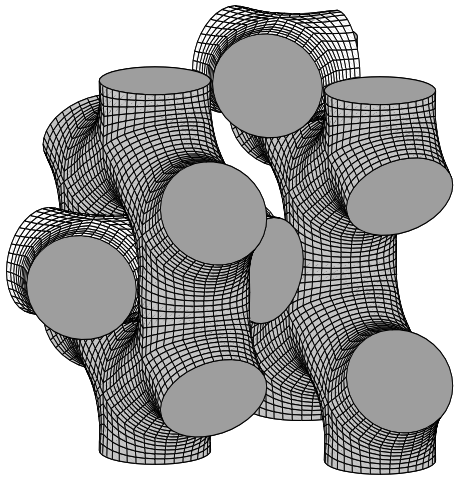

Figure 18: Unsuccessful attempt to fill space with the 3-armed surface.

The space filling arrangement of this surface requires more ingenuity. Obviously, we have already encountered the solution: The network arranges in space group $Ia\bar{3}d$ [78]. Viewed along coordinate axis (Fig. 19 left), the structure composes of two sets of connected spiral networks. All the rods are oriented along the face diagonals. A better perspective is to view along the face diagonals (Fig. 19 right). From this angle the A and B regions are seen to create alternating layers of hexagonal networks, which pierce through the neighboring layer and connect with the next layer in the sequence. Thus we can once again ascertain that partitioning into two subvolumes with same connectivity occurs. The unit cell contains no less than 16 basic surfaces. When the volume of each basic block is $\sqrt{2}$, the two networks fill the space completely divided

by Schoen's G minimal periodic surface, which is quite impossible to visualize.

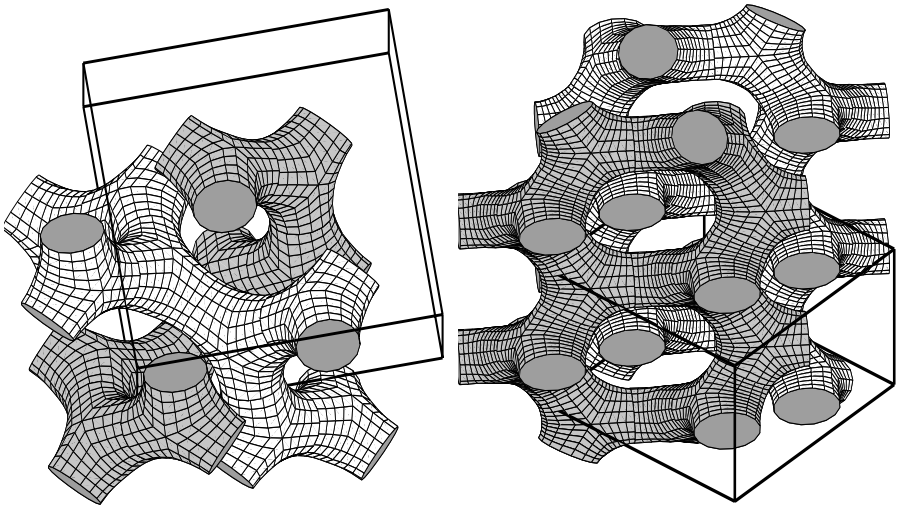

Figure 19: Two different perspectives of the G surface. The structure on the left also gives the unit cell.

Properties of the minimal surfaces. In the bicontinuous structures of aqueous surfactant solutions, the surfactant forms a bilayer whose center is at the minimal surface[23]. The grey and white networks in figures 14, 16 and 19 would then correspond to two unconnected water channels, and the space in between is occupied by the surfactant. For a nonzero surfactant volume fraction ϕ, the surfactant/water interface cannot obviously be minimal. Thus the interface is either assumed to lie at a constant distance $\pm D/2$ from the minimal surface, or two constant mean curvature surfaces enclosing volume fraction $(1-\phi)/2$ are generated *e.g.* with the method described above. In either approach a slight frustration is created: In the constant thickness model the surface area is not at minimum, while using the minimum area surfaces the surfactant molecules have to conform to layer of non-uniform thickness. However, this frustration is smaller than in both lamellar and (inverse) cylindrical phases and therefore it is suggested to be the energetic term responsible for the formation of cubic structures in between [121, 122]. The addition of hydrophopic molecules will decrease the frustration [122] whereas large frustration is expected for chains with low flexibility [123].

Any surface minimizing area per volume must have constant mean curvature H. It follows that at the symmetrical case $\phi = 0.5$ the curvature vanishes exactly. This property defines the minimal surface. If we move any surface by an amount L along the surface normal, the area element changes by

$$dA' = \left(\frac{L}{R_1}+1\right)\left(\frac{L}{R_2}+1\right)dA = \left(KL^2+\frac{1}{2}HL+1\right)dA. \qquad (92)$$

[23] In ternary systems, either oil or water phases may constitute this layer.

In particular, starting from the minimal surface the displaced surface area is

$$A = A_0 + L^2 \int_{A_0} K \mathrm{d}A = A_0 + 2\pi\chi L^2, \tag{93}$$

where χ is the Euler characteristic of the surface. This is a (negative) whole number obtained from

$$\chi = 2(1-g) \tag{94}$$

where g is the genus (number of holes) in the surface. Thus it does not depend on the actual surface area, but takes a specific constant value depending on what is the connectivity of our basic surface block. For n-armed block $\chi = 2 - n$.

Surface	space group	χ	ς
G	Ia3d	-8	3.091
D	Pn3m	-2	1.919
P	Im3m	-4	2.345

Table 1: Properties of the minimal surfaces. The values of ς are taken from [124] and may be seen to correspond to maxima in Fig. 13 with appropriate unit cell size.

The surface area per repeat unit scales as $A_0 = \varsigma a^2$, which defines another dimensionless parameter particular to given type of minimal surface. Integrating Eq.(93) we get a relation

$$\phi = 2\varsigma \left[\left(\frac{L}{a}\right) + \frac{2\pi\chi}{3\varsigma} \left(\frac{L}{a}\right)^3 \right] \tag{95}$$

between the volume fraction ϕ, the length of surfactant (equal to L) and the size of the unit cell a. This can be used to assess the structure determination.

The specific surface is

$$S/V = \frac{2\phi}{D} \left(1 + \chi \frac{\pi\phi^2}{2\varsigma^3}\right) \tag{96}$$

where D is the bilayer thickness. Since χ is negative, the surface actually has smaller specific area than in the lamellar system albeit by only a few percent. If the surface favors inward curvature of the bilayer (toward water), the system could favor the ordered cubic structure in spite of the loss in entropy required to form a periodic surface. The inward curvature is controlled by the temperature; increased temperature increases the chain splay and thus the curvature, typically by 0.5 % per $\circ$C [125, 126].

Transformations between the phases. Though the basic membrane theories are able to justify the existence of the bicontinuous cubic phases, still a lot remains unknown. Recently, interest has been directed to structural transformation between these phases.

A full sequence of phases has been observed in fatty acid/phosphatidyl choline mixtures[24] in water [94]. The transitions follow sequence H_{II} $\rightarrow$G$\rightarrow$D$\rightarrow$P in increasing water content (between 0.3–0.5). Most notable variable is the unit cell size, which according to Eq.(95) should be proportional to $a \sim \varsigma$ for constant ϕ, L and K. The ratio of quantities a/ς are said to be 1:1.022:1.07 respectively [127]. The

[24] Lauric-,myristic-,palmitic- and steric acids with DLPC, DMPC, DPPC and DSPC phospholipids in 2:1 composition

above phase sequence has been predicted by the calculation of the elastic energy in the constant mean curvature model [126].

The pathway from one IPMS to another is obtained by systematically linking the junctions of the bicontinuous labyrinths [128]. Recently Fogden [129] was able to show that the pathways could also be traced using minimal surfaces. Thus the intermediate states would not be as energetically unfavorable as in the labyrinth net models. As the routes are created using rhombohedral and tetragonal distortions, this is also offered as an explanation for observations of these symmetries [123, 78, 82, 89]

Practical phase determination. The past of cubic phase determination is marred with misassignments, so this seems like a perfect place to bring up the subject of experimental difficulties in phase determination.

The major problem is the same as with the lamellar and cylindrical phases; there are generally too few reflections to be seen for definite phase determination. Number of observed reflections is higher in cubic systems because of the more 'solid' nature of the matter, but so is the number of possible structures.

The first thing to do is to find enough reflections to assign correct crystallographic space group(s). This has some pitfalls. An occasional reflection may be absent or almost absent due to minimum in the structure factor though it may be allowed by the space group. For the lamellar and to an extent the cylindrical phase, a powerful method is to make scans with different dilutions to reveal these minima. This has limited application to cubic phase because these appear in a narrow composition range.

Second difficulty lies in the tendency for samples to grow large crystals or the tendency to orient with shearing or influence of the sample cell walls. This will result in false structure factor data if the powder diffraction technique is used. The sample can be powderized by repeated annealing-quenching cycles [79, 98]. On the other hand, large mesomorphic 'single-crystal'-domains might also be produced with thermal treatment [98, 130] or with shearing [131]. Single crystals help tremendously in solving the crystal structure and are also useful if diffuse scattering (peak shape) analysis is tried [132, 130].

A third problem is that cubic phases are often metastable and occasionally a number of different phases may coexist [93]. It is common that cubic structures formed at elevated temperatures may preserve for months [87] in room temperature. It may thus be difficult to decide which are equilibrium structures [133].

Few attempts have been made to obtain density maps, in other words, to relate the observed intensities to the contents of the unit cell. Most notable efforts are those by Mariani [100]. In the early days, structure factors were calculated by modeling the networks with connected lines or rods and the results thus obtained were fair.

For the case when the surface is defined and surrounds a homogeneous region, the structure factors are most conveniently calculated as a surface integral [59, p.104]

$$F(\mathbf{k}) = \frac{i}{k^2} \int_A e^{i\mathbf{k}\cdot\mathbf{r}} (\mathbf{k} \cdot \mathrm{d}\mathbf{S}). \tag{97}$$

If the surface is further approximated with facets, the integral can be reduced to summation

$$F(\mathbf{k}) = \sum_n^{\text{facets}} \frac{\mathbf{k}\cdot\hat{\mathbf{s}}_n}{k^2 k_n^2} \sum_j^{\text{edges}} l_{nj} \left(\mathbf{k}\cdot\hat{\mathbf{v}}_{nj}\right) e^{i\mathbf{k}\cdot\mathbf{c}_{nj}} \frac{\sin \mathbf{k}\cdot\mathbf{l}_{nj}/2}{\mathbf{k}\cdot\mathbf{l}_{nj}/2} \tag{98}$$

where the first sum runs over all flat phases, $\hat{\mathbf{s}}_n$ are unit vectors normal to these surfaces and $\mathbf{k}_n$ is the component of scattering vector $\mathbf{k}$ at the surface plane. The second sum is over all surrounding edges $\mathbf{l}_{nj}$ (ensure of the correct direction of circulation), $\mathbf{c}_{nj}$ are the middle points of the edges and $\hat{\mathbf{v}}_{nj}$ are unit vectors perpendicular to both $\mathbf{l}_{nj}$ and $\hat{\mathbf{s}}_n$.

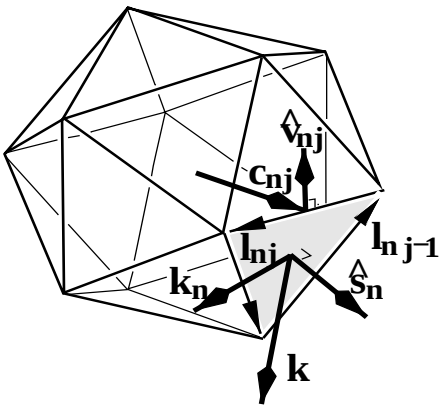

Figure 20: Illustration of Eq.(98) for the calculation of scattering factor.

For example, Fig. 21 present scattering intensity for binary AOT/water system with water content $\phi_w = 0.2$. The data is again taken with the conventional setup at HU. The reflections are easily assigned to the $Ia\bar{3}d$ space group. However, the forbidden reflection (411) occurs as suspiciously powerful. As the sample is slightly into the two phase region between 16 % and 22 %, the extra reflection is due to coexistent hexagonal phase. There is a well known epitaxy between the $Ia\bar{3}d$ and hexagonal phases, where the reflections (211), (411) and (422) transfer into (10), (11) and (20) reflections respectively at *exactly* same positions [134]. The occurrence of hexagonal impurity has been known to destroy analysis before [103].

The remaining reflections are found to decrease fast with respect to the scattering angle, contrary to any plausible model (*c.f.* Table 2). An additional Gaussian thermal factor is needed to make experiments and models agree [78, 79, 100].

For poorly ordered systems, the intensity curve shows just one broad maximum. Then recognition of the phase is impossible without additional knowledge. Such knowledge is provided *e.g.* by the Porod law. If there exist sufficient phase segregation and the Porod region in the intensity curve is found, the normalized and slit corrected intensity follows the form [135, 136]

$$I(k) \simeq \frac{2\pi S}{k^4 V}\left[1 + \frac{3}{8}\left(H^2 - K/3\right)k^{-2} + \mathcal{O}(k^{-4})\right], \tag{99}$$

where S/V is the specific surface [9]. The mean and gaussian curvatures, H and K, here stand for their averages over the whole sample. Thus when the two first terms in Eq.(99) can be determined and with the knowledge of the structural length scale for the only reflection, the different morphologies may in principle be distinguished [136].

hkl	S_1	S_2	S_3	S_{obs}	q^2_{hkl}	q^2_{obs}
211	100	100	100	100	6	6.04
220	7.5	13.9	16.1	41.4	8	8.07
321	2.5	13.2	0.0	1.3	14	14.16
400	3.7	7.9	0.0	0.9	16	16.02
411*	0	0	0	9.2	18	18.00
420	10.2	10.5	3.7	2.7	20	20.09
332	12.2	38.7	0.7	0.6	22	21.98
422	3.3	6.3	0.5	1.4	24	23.90
431	1.4	3.8	0.0	1.1	26	26.02
521	0.6	1.0	2.1	0	26	-
440	0.4	1.9	4.8	0.1	32	33.17
532	0.1	7.1	10.7	0	38	-
611	0.0	16.3	24.7	0.5	38	38.81

Table 2: Observed intensities (peak areas) for the diffraction curve in Fig. 21. The calculated intensities are based on constant mean curvature surfaces; for S_1 a two phase model is used with $\phi_w = 0.2$, for S_2 a three phase 'vesicle' model with additional 2.4 Å thick hydration layer [110] and for S_3 a similar model with the AOT and water phases inverted. Reflection marked with asterisk is not allowed by the $Ia\bar{3}d$ symmetry. Model intensities are corrected for multiplicity of reflections.

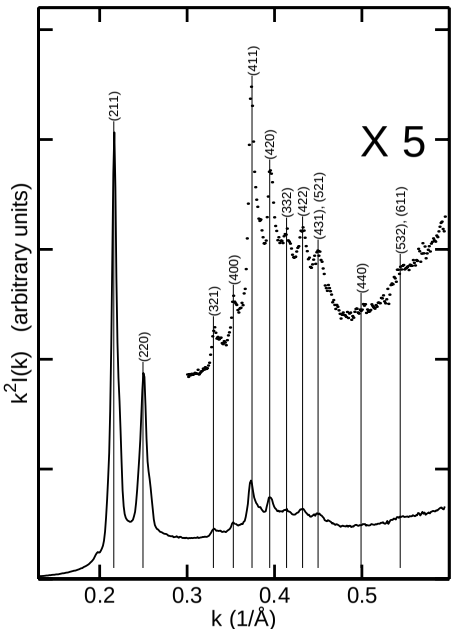

Figure 21: Scattering intensity for AOT/water mixture at 20 % water content. Vertical lines correspond to reflection positions for a cubic unit cell with cell size 71.2 Å. The intensity curve is corrected for isotropic orientation of the sample.

Polymers and surfactants

We arrive now at the theme of this thesis which is the phase formation of surfactants with associating polymers. The polymers contain either anionic or cationic sites for the surfactants to complex with. Due to the charged groups, the polymers are also referred to as *polyelectrolytes*[25]. As was the case with surfactants, the polyanions contain acid derivatives (*e.g.* sulfonated polystyrene) and polycations are either amines (P4VP) or ammonium salts (cationic starch). The polymer is complexed with associating amphiphile to form a mesophase. An exception is Poly(styrene sulfonate) in Paper I which is only studied in the ionomer state (for a low degree of sulfonation it may be considered as an amphiphile).

One may thus picture the polymer replacing water in the previous case of aqueous surfactant systems. The important difference is that the hydrophilic sites are now connected by the polymer backbone. This has a two way effect: 1) It enhances the formation of lyotropic phases by this confinement and (in case of polyelectrolytes) the charge neutralization. 2) The attached surfactants change the conformation of the polymer backbone which again is the objective goal of most of this work. A flexible polymer forms a gaussian coil in solution — a scarce bundle, whose straightening requires a grand decrease in entropy. This is balanced by the enthalpy available from the polymer/surfactant bonding. Thus polymer conformations may be turned into

[25]Polymer with both positive and negative charges is also called *polyampholyte*

sheets or tubes depending on the superimposed morphology of the surfactant. This opens a wealth of possible applications [137].

In way of examples, a single polymer chain in solution may be condensed or folded into a compact particle. Certain gene therapy treatments rely on successful transfer of the DNA, which is a bulky anionic macromolecule, into the cell through its protective membrane[26]. The use of cationic lipides for DNA condensation and the interaction of these liposomes with the cell membranes is an active field of research [138]. The membranes themselves are complex combinations of various lipids and proteins [61] and the cell regulates its function by controlling the lipid composition which directly effects the way the lipids pack in the membranes. Similar condensation may be applied to a whole network of cross-linked polymers in a phenomenon known as polymer network collapse. Cross-linked polymers swell in solvent and may absorb water several hundred times their own weight. Addition of certain agent (or change of temperature or pH) may result in sudden stepwise decrease in the gel volume [139]. Similar effect by surfactants on slightly cross-linked polyelectrolyte gels has recently been demonstrated [140].

Polyelectrolyte surfactant solutions. The presence of the polyelectrolyte in a solution of oppositely charged surfactants has the tendency to lower the critical micellar concentration [141]. This is simply due to increased surfactant concentration surrounding the polymer chain. At the same time, the overall charge of the chains decreases due to charge neutralization and the polymer can adopt a more compact conformation. Ultimately, the complex precipitates from the solvent and forms a dense neutral phase with 1:1 stoichiometry [142]. This phase still contains appreciable amounts of the solvent in addition to the complex[27]. These complexes exhibit a rich variety of forms. Hexagonal and cubic structures are common. The bicontinuous cubic phases are not observed. Typical structures are the $Pm\bar{3}n$ (223) (this appears to be quite similar to the surfactant/water case so perhaps this suggests that the closed micelle model is more appropriate), fcc and hcp [140].The $Pm\bar{3}n$ and hcp structures are observed in Paper II of this thesis.

Polyelectrolyte surfactants in the solid state. When the solvent is evaporated, ordered structures of polyelectrolytes and amphiphiles may form. Recently these have received greater interest (for reviews, see [143]) The predominant morphology is still lamellar [144]. In several occasions the lamellar form is deformed with periodic undulations or perforations [145]. The layers stack systematically, so that the undulations arrange in cubic of rhombohedral (*e.g.* Fig. 18) structures [146]. In cylindrical micelles, similar "lumps" may packed in cubic form [147].

The major reason for the dominance of lamellar phases may be the as yet relatively limited group of different samples that have been tried in comparison with the 'no-polymer' case. Specifically, the surfactant has often been aliphatic.

Studies of polymer/amphiphile[28] complexes in varying interaction. It was suggested that even flexible polymers with sufficient amount of surfactant yield mesophases in a good solvent to the side groups [148]. In the first experiment, this was tested using two different forms of poly(vinylpyridine) (P2VP and P4VP) in

[26] Currently, viruses are applied to the job and there is call for equally effective means but without the immunological hazards to patients

[27] In many occasions the polymer and surfactant are dissolved as salts, so the system is more complicated still as it contains four ionic species which are capable of forming four different neutral salts in the mixture.

[28] "Amphiphile" is used instead of "surfactant" which is a term strictly reserved for water soluble amphiphiles.

xylene solvent [149]. Liquid crystallinity was indeed observed, though not attributed to the presence of the solvent.

Next we tried different forms of interaction. In this respect P4VP was also a very versatile polymer. It can be protonated with a strong acid such as DBSA [149], coordination complexed with a transition metal [150] or hydrogen bonded [151]. In addition, the pyridine group can be first "doped" or protonated with *e.g.* methanesulfonic acid (MSA) prior to hydrogen bonding [152]. Some of the early observations concerning the required interaction are collected in Paper III.

Ordering transition in hydrogen bonded polymer/amphiphile systems. The most striking property of some of the hydrogen bonded systems was their ability to show a sharp ordering transitions. Below the ordering temperature, the SAXS intensity showed a very sharp reflection quite unlike in any other system scanned so far. Paper IV deals with this transition. It was designated as the *order-disorder transition* (ODT), a concept borrowed from block copolymer theory [153] (subject of the next section). Thus this would be the first observation in comb-coil polymers but it is known in liquid crystalline side chain polymers (LCSCP's) [154]. The side-chain crystallization observed here is also a common event in LCSCP's.

In block copolymers at ODT, the system goes from homogeneous to microphase separated state. Same conclusion may be drawn in the present case from that the transition is accompanied by the appearance of optical birefringence. The ODT in blockcopolymers is weakly first order and also here it gives a small exothermic peak in the differential scanning calorimetry (DSC). Some things are not that analogous; in this system the transition seems to be limited to hydrogen bonded amphiphiles. The essential property of the hydrogen bond is its relative weakness, thus the bonds are constantly created and broken by thermal motion. Block copolymers, on the other hand, are permanently attached by covalent bonds.

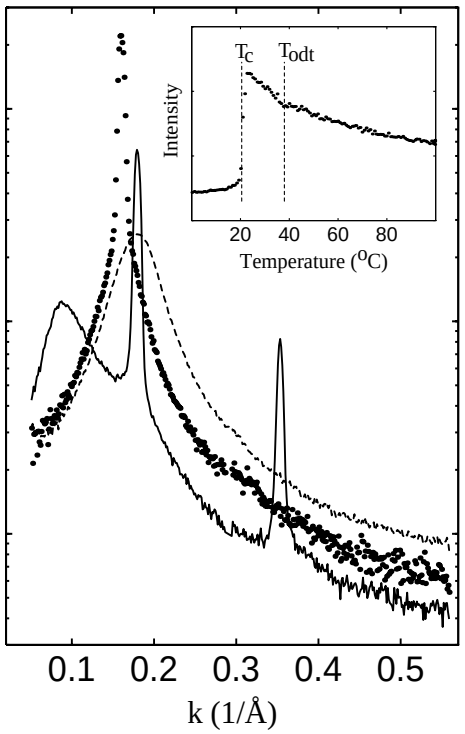

Figure 22: Scattering intensity of $P4VP(PDP)_{1.5}$ at three different forms distinguished by the crystallization temperature T_c and the order-disorder transition temperature T_{odt}. Solid line: $T < T_c$, dots: $T_c < T < T_{odt}$, dashed line: $T > T_{odt}$. The insert shows relative intensity under the main reflection at $k = 0.16$–0.18 Å^{-1}.

In SAXS, the ODT is characterized by discontinuous changes in the maximum intensity and peak width. These are exhaustively reported [155]. Let us still reproduce the scattering intensity of the $P4VP(PDP)_{x=1.5}$ system as it serves as textbook example of lamellar systems discussed so far. This system shows both disorder transition and crystallization at slightly lower temperature. Figure 22 shows scattering intensities in logarithmic scale within each three regions. Across the ordering transition (dash to dot) at T_{odt}, the *integrated* intensity (in-

set) is continuous (true for $x \geq 1$). This indicates loss of LRO without reorganization of the structure at the molecular level. In essence, the fluctuation amplitude remains constant at the ODT. The crystallization (dots to line) entails a collapse of the "neat" end-to-end formation of atactic PDP chains into an interdigitated crystalline packing. This slight densification of one layer causes immediate jumps in both quantities. On crystallization, the second order reflection, almost totally missing before, becomes clearly visible. Also, the first order reflection is more like a crystalline reflection whereas above T_c it has the familiar tail akin to the 'quasi-periodic' LRO encountered previously. The dynamics of the two cases are totally different; the mesoscopic phase has flexible polymer chains undergoing constant motion whereas in the second case the chains are effectively anchored by the crystallized tails of the PDP sidegroups.

Liquid crystalline polymers. Above we have followed the route from polyelectrolyte-surfactant complexes to non-ionic liquid crystalline polymer/amphiphile systems. There is another vast field of research, which has come to use similar ideas – that of polymer liquid crystals (PLC). In the traditional PLC architecture, the polymer is covalently attached to a mesogenic group via a spacer group. This is the *side-chain liquid crystalline polymer* (SCLCP), a type of polymer which due to its form is also called *comb-like polymer*. Recently, this field has also progressed to supramolecular concepts replacing the noncovalent interactions with ionic bonding, hydrogen bonding etc. These might be applied in either the main-chain polymer [156] or the side chain group [157].

Block copolymers

The type of phase segregation found in surfactant/water systems also occurs between dissimilar polymer chains[29]. Perfect analogy with amphiphiles is met in block copolymers[30] where the chains are connected with covalent bonds, thus again preventing macro phase separation. Consequently, block polymers exhibit the same properties as amphiphiles, from being solubilizers and surface active agents for selective solvents and homopolymers[31] to forming micelles, emulsions and ordered phases [158, 159]. From the theoretical point of view they are more ideal to study phase behavior than their "molecular" counterparts since *e.g.* the mean-field picture is better valid for such large molecules [160]. From the materials synthesis side, the huge choice of chain architectures has led to a number of exotic ordered morphologies.

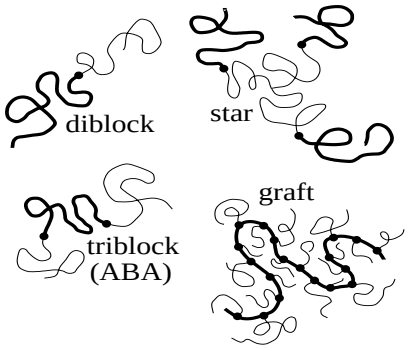

Figure 23: Various block copolymer chain architectures.

[29] Even between polymers made of the same monomers but differing in chain length N

[30] *Copolymer* contains two or more different monomers, which in *random copolymers* are in random order and in *block copolymers* constitute sequential blocks of the same monomer.

[31] *Selective solvent* is the one that dissolves one block only the opposite of which is *neutral solvent*; *homopolymers* are the blocks without the covalent bond between them.

Order disorder transition in diblock copolymers. Most attempts to understand block polymer behavior naturally concentrates on the most simple form, *i.e.* the *diblock* copolymer (see Fig. 23). The formation of ordered domains is governed by the volume fraction ϕ of the blocks. We can predict the following phase

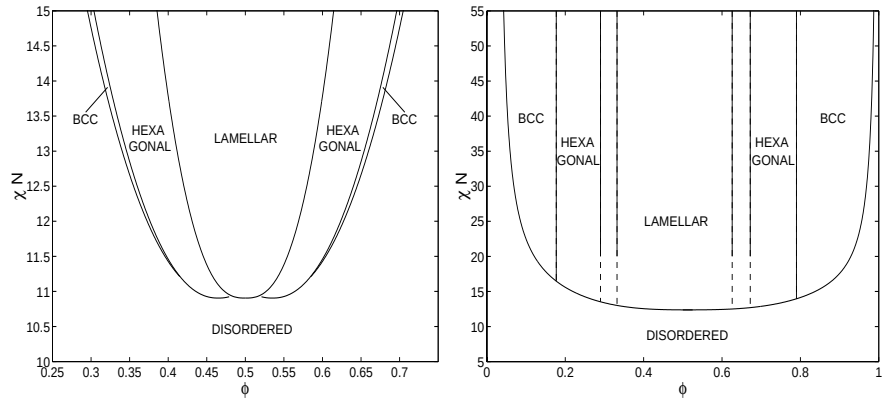

Figure 24: Left: Theoretical phase diagram for a symmetric diblock near $\phi = 0.5$ as first considered by Leibler [153] and later corrected for fluctuation effects by Fredrickson and Helfand [161]. In the symmetric case, the disordered to lamellar transition is predicted to vary as $(\chi N)_{ODT} = 10.495 + 41.022 N^{-1/3}$ Right: Actual experimental phase diagram for PS-PI [163, 164]

sequence [153, 161, 162] as given in Fig. 24. The lowest curve outlines the order-disorder transition temperature, the interaction parameter generally depending on temperature as $\chi = \alpha/T + \beta$. The difference between Leibler's theory [153] and Fredrickson-Helfand [161] theory concerns the disordered phase near ODT. In the former theory, the blocks are completely mixed and only weakly perturbed from the gaussian chains. Thus domain spacings should scale with number of monomers N in the polymer chains as $D \sim N^{1/2}$ though in this picture domains do not exist above ODT temperature. However, the structure factor contains a maximum due to correlation hole effect[32]. In the latter theory, the fluctuation amplitudes are comparable below and above the ODT. Both should be considered as microphase separated states and the chains are expected to stretch out to give $D \sim N^{\delta}$ where $0.7 < \delta < 0.8$ [165]. The disordered phase is said to resemble the late stage spinodal form [164]. Crossover to the mean field region (stretched to Gaussian chain) is expected to occur at temperatures much higher than ODT.

The nature of ODT has invoked numerous scattering studies, the outcome of which confirm the Fredrickson-Helfand theory [165, 166]. There is an inherent problem in that the polymer length should not be too large in order to have a feasible transition temperature. On the other hand experiments have been carried out with very short polymers with high incompatibility (high χ) [167]. The ODT in block copolymers is not as easily seen as it was in *e.g.* Fig. 22 when conventional x-ray sources are used.[33] Measurements are feasible with synchrotron radiation sources [168] and results have shown marked analogy to the studied polymer/amphiphile system.

[32] Deficiency of close contacts between blocks of type A due to the presence of the connected block B and vice versa.

[33] SANS is not very useful either as it has poor energy resolution.

Ordered phases of block copolymers. The preference of one morphology over the other follows the same principles as in surfactant/water systems. These include preferential chain length and surface area for a given diblock and the desire to find surface of constant mean curvature, resulting in inevitable frustration to fill the volume with these constraints. There is an important addition to energetics involving the stretching of the polymer chains which now are much longer than the 10-18 units in case of the amphiphiles. By nature, a flexible polymer is in the form of a random coil whose length grows *less than* linearly with N and consequently its cross section increases with N. Forcing an asymmetric ($N_1 \neq N_2$) diblock copolymer in a lamellar morphology requires stretching of the longer block to make the cross sections equal (*c.f.* Fig. 25). Thus there is a tendency of curvature toward the shorter block. By considering just this effect in one can generally deduce that lamellar morphology is preferred between $0.3 < \phi < 0.7$, cylinders appear at minority volume fraction around $\phi = 0.25$ and below that saddle shape surfaces (*e.g.* bicontinuous structures) are favored [169].

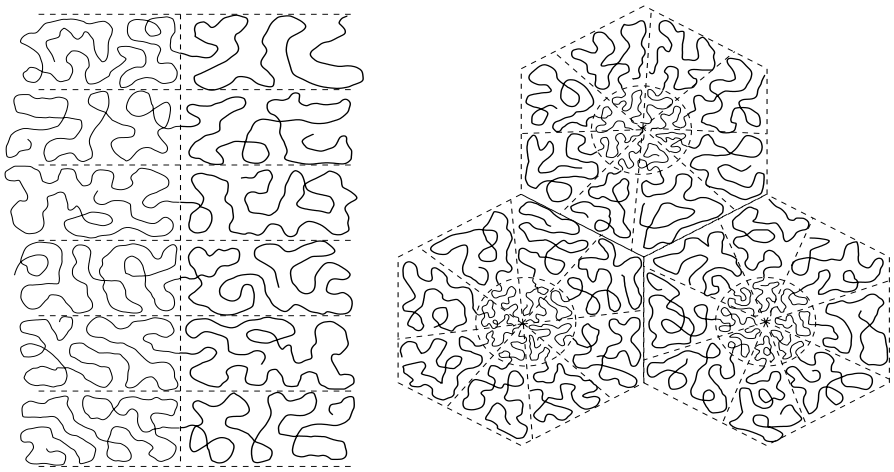

Figure 25: Packing of diblock polymers within the lamellar and cylindrical phases. The frustration in latter means that if the phase boundary follows the minimal surface (cylinder), the chains along the hexagonal corners have to stretch more to ensure constant density.

The actual phase transition compositions (Fig. 24) are slightly different. Note that the lines separating the ordered phases run practically vertical, *e.g.* there are no phase transitions as a function of temperature except for a narrow composition window between the lamellar and hexagonal phases. The new phases are found near the ODT line (marked by the dashed line). They include, in increasing temperature[170], hexagonally perforated layer (HPL) [171], hexagonally modulated lamellar (HML) (these two are already familiar from polyeletrolyte/surfactant systems) and the gyroid [172] (based on the G-surface as in surfactant systems). At low temperatures, the lamellar phase is usually retained and is expected to be more and more favorable [173]. The composition window is narrower, the higher the molecular weight [167], which may be due to diminished fluctuations with higher N[165] so the appearance of the phases is more related to the polymer length and is possibly richer for short polymers [174].

The ordered phases get more complicated in *e.g.* ABC triblock copolymers where each block constitutes a different phase [175]. Perhaps more interesting are diblock copolymers synthesized to *starblock* or *graftblock* form (Fig. 23), where a number of identical diblock arms are linked to a common center. These where the first where the gyroid morphology was seen [159, 176] though not identified as such before similar structures were first observed in linear diblock copolymer melts [172, 177]. Originally [176] the gyroid was first mistaken as the double diamond (D-surface) structure and it is still not clear whether other bicontinuous phases are found in diblock copolymer melts [178].

Contrary to the polymer/amphiphile systems[34], the structures found in block copolymers can be fairly easily imaged directly using electron microscopy. Compared with the scattering techniques, the EM provides a very detailed picture, albeit from a tiny volume, as opposed to the "statistical" information obtained by SAXS. To illustrate the gap between microscopic image and scattering, consider the Fourier transform of the faked EM images in Figure 26. For creation of such images, there is an extremely

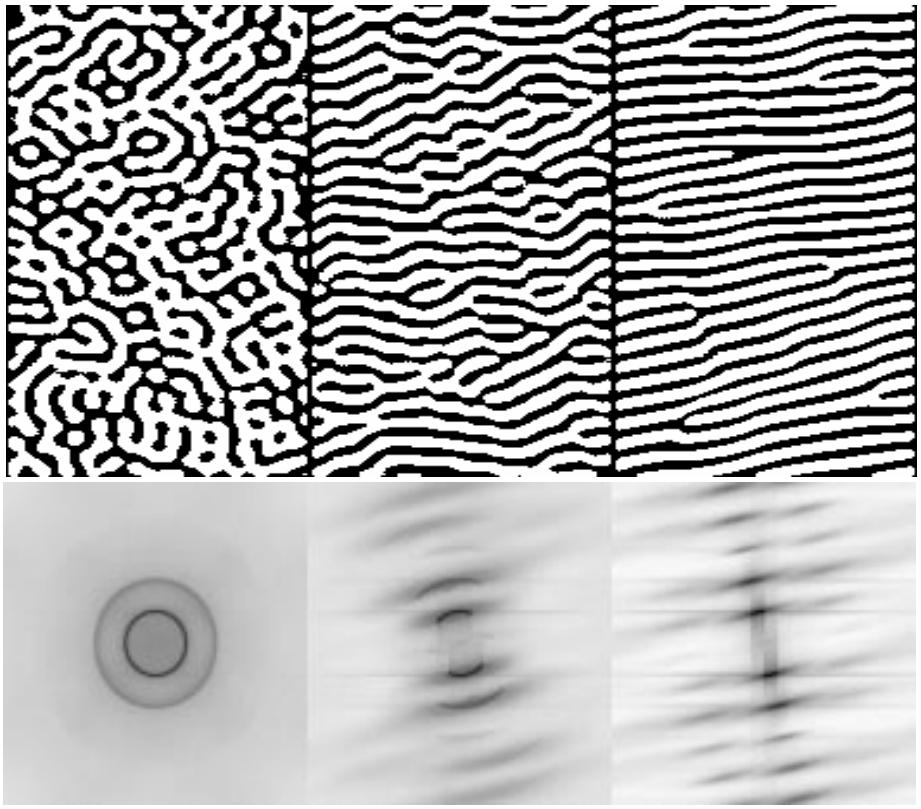

Figure 26: Computer generated images of two phase lamellar system with variable orientational distribution. Below is their respective scattering functions. The direct images show only a portion of the pattern from which the intensity is calculated.

[34] The spectacular pictures by J. Ruokolainen [179, 180] are rare examples of polymer/amphiphile microstructure ever been imaged.

simple algorithm by Cahn [181] who used it to mimic patterns of late-stage spinodal decomposition and which has also been applied for modeling bicontinuous microemulsions [182]. In this method we superimpose a number of waves

$$G(\mathbf{r}) = \sum_j \cos\left[\mathcal{R}(\mathbf{k};\varphi_j)\cdot\mathbf{r} + \phi_j\right] \tag{100}$$

where $\mathcal{R}(\mathbf{k};\varphi_1)$ denotes rotation of a fixed wavevector $\mathbf{k}$ by a random angle (or set of angles), φ_j and ϕ_j are random phases. The density is then assigned a binary value by the output of condition $G > 0$. In the leftmost frame, $\mathbf{k}$ takes random orientations whereas in the center and right frames the angular range in limited to 70 and 20 degrees respectively. Thus the first case resembles images of spinodal decomposition whereas the rightmost frame is not unlike magnified portions of images from truly lamellar morphologies (compare, for example, to [179, Fig.5]) complete with the edge dislocations.

The angular range which was used to create the real-space images is clearly seen in the scattering patterns. The higher order reflection rings are obviously created by the binary clipping process[35]. Through analysis of isotropic scattering functions obtained by angle averaging of the figures one would deem each example as merely "lamellar". It would be extremely difficult to distinguish between orientational disorder as pictured here and other effects such as thickness variation (*e.g.* created by allowing variable values for $\mathbf{k}$) and diffuse interfaces.

By further underscoring the difference, imagine that the waves are generated to follow hexagonal symmetry (Fig. 27). With sufficient randomness the hexagonal symmetry is far from obvious in the direct image and microscopically the structure bears close resemblance to the spinodal. Yet, the scattering intensity obtained from this pattern has distinct diffraction spots according to the hexagonal symmetry.

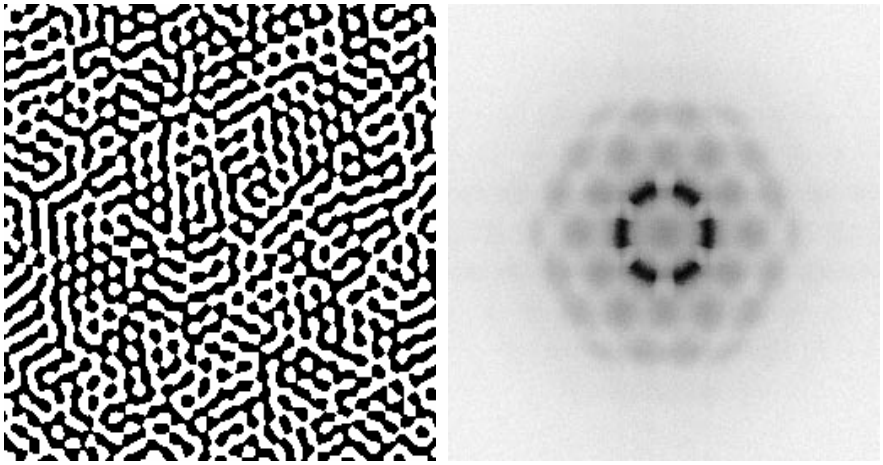

Figure 27: Computer generated image where the density waves are generated according to a six-fold symmetry (left) and the resulting diffraction image (right).

[35] Note that the original lamellae have been skimmed to fill approximately 1/3 of the volume which is why orders $3n$ are damped instead of $2n$.

Block polymer structure factors. The structure factor for the disordered state was given by Leibler in his mean field theory[153]. The calculation is based on the random phase approximation (38) extended to incompressible two phase system consisting of ideal polymer chains and interaction between neighbors given by χ,

$$S(k) = \frac{|S_{ij}|}{\sum_{ij} S_{ij} - 2\chi |S_{ij}|} \tag{101}$$

where S_{ij} are the partial structure factors and $|S_{ij}|$ denotes matrix determinant. This is the general form. For diblock copolymers the matrix elements are given as [153]

$$\begin{aligned} S_{11} &= N g_1(\phi, x) \\ S_{22} &= N g_1(1-\phi, x) \\ S_{12} = S_{21} &= \tfrac{N}{2}\left[g_1(1,x) - g_1(\phi,x) - g_1(1-\phi,x)\right] \end{aligned} \tag{102}$$

where g_1 is the Debye function

$$g_1(\phi, x) = \frac{2}{x^2}\left[\phi x + e^{-\phi x} - 1\right], \qquad \text{with } x = \frac{N}{6} k^2 a^2 = k^2 R_g^2 \tag{103}$$

Thus the reciprocal of structure factor

$$S^{-1} = F(x, \phi) - 2\chi \tag{104}$$

has temperature dependence through the interaction parameter χ only. The fluctuations (Fredrickson-Helfand theory) are introduced by substituting for the interaction parameter a renormalized parameter [162]

$$\chi_{\text{eff}} = \chi - \frac{vC(\phi)}{2a^3 N^2}\left[F(x^*, \phi) - 2\chi_{\text{eff}}\right] \tag{105}$$

where $C(\phi)$ is a composition dependent constant, v is segment volume and x^* is related to wave vector of the fluctuations. The principal result of this theory is that the inverse of the structure factor no longer has the $1/T$ dependence. This is chiefly the argument on which experimental confirmation of the fluctuation model is based.

Scattering studies of ordered phases have been used successively for structure determination. Apart from this, one may obtain limited information on the microdomain size and domain boundary width [183]. Information on polymer segment as well as solvent distributions require phase contrast techniques and are therefore more readily performed with neutrons [184].

Liquid crystalline block copolymers. An increasing area of interest is to introduce a competitive organization to the microphase separation of polymer blocks within one or several of the blocks. Such competition takes place in *e.g. rod-coil copolymers* where the "rod" part is a rigid sticklike polymer which has a tendency to form orientationally ordered structures [185]. There is thus mesophase formation at completely different length scales, and we therefore speak of *hierarchial structures*. The semicrystalline ionomers which are dealt with in Paper I are also a crude form of hierarchial structures though they do not show such self organization as is the key issue here. Paper V studies PS-*block*-P4VP(PDP)$_{1.0}$, which is a perfect example of such concepts. It represents *liquid crystalline block copolymers* which also have been reviewed intensively during the recent years [186]. Specifically we are dealing with

a LC side group block copolymer. The liquid crystalline block is again P4VP with hydrogen bonded PDP sidegroups and the coiled block is polystyrene. Strikingly, the P4VP/PDP regions seem capable of forming macrophase separated lamellar morphology within lamellar, cylindrical or spherical domains and allow also the formation of similar inverse domains of PS in lamellar P4VP/PDP matrix [180]. The PDP chains orient along the block-block interface which is discernible in the TEM images [180]. Same conclusion may be drawn from the recent SAXS measurements on macroscopically oriented samples [187]. These show that the reflections from the LC structure and block copolymer structure occur at right angles to each other [188].

The temperature behavior of the system is studied in Paper V, and the results indicate independent transitions within both blocks. They seem strangely uninfluenced by the presence of the other block and the confinement to the microdomains. Thus P4VP/PDP exists in the side chain crystalline, lamellar and isotropic forms with due transitions observable in the SAXS patterns and PS has glass transition temperature at about 85°C. None of the samples that have been measured show order-disorder transition of the block structure. It may be that at the temperature near the ODT, the electron density contrast is already too weak to be seen in SAXS. At high temperatures PDP is gradually disassociating from P4VP. At about same temperatures, the PS becomes soluble in PDP, *i.e.* PDP changes from selective to neutral solvent. This in fact is sufficient to induce an order-order transition [152] if the composition lies close to coexistence line[36].

Summary of the papers I–V

Paper I. The first paper is a result of collaboration with the Laboratory of Polymer Chemistry. The aim of this project is to find a cheap and effective means of producing proton conducting films from commercial films. A series of proton exchange films have been prepared with irradiation techniques and characterized in our laboratory with x-ray scattering techniques [189], with both small angle and wide angle. The present paper present results obtained with a relatively novel technique of anomalous scattering (ASAXS). The measurements were carried out at Hamburger Synchrotronstrahlungslabor (HASYLAB). The author was responsible for both experiments and data analysis. The objective of this work was to learn more about the distribution of the proposed ionic aggregates within the styrene grafted poly(vinylidine fluoride) (PVDF) films. The analysis was able to show that the prepared films were organized in a two-level phase separated structure. The sulfonated grafts are incorporated in the amorphous part of the semicrystalline polymer matrix. The results indicate that it organizes there in a layered form of the hydrated polysalt. It is discussed that water uptake disrupts this structure and again water filled micelles form.

Paper II. The subject of the second paper bears also familiarity of Papers III-V, in that it deals with attempts to change the conventional polymer conformation by interaction with functional surfactant molecules. In this work, however, the polymer is a very hydrophilic polyelectrolyte cationic starch (CS) and the small angle measurements are carried out of precipitated complexes obtained from aquous solutions. The precipitants are prepared at the University of Technology, by our collaborators at the Department of Forest Products Technology. The measurements

[36] The P4VP in this work was protonated with MSA

were carried out at HU by myself and Mr. Teemu Ikonen.

The structures were investigated with various surfactants, varying charge density and neutrality of the solution. Ordered and disordered micellar complexes were formed. The requirement for the ordered complexes could be outlined in terms of sufficient charge density and neutrality. The ordered structures included hexagonal, hexagonal close packed (hcp) and micellar cubic ($Pm\bar{3}n$) forms.

Paper III. Papers III to V represent cooperation with the Polymer Physics group from Materials Physics Laboratory at the University of Technology and their subsequent collaborators. They have studied polymer/amphiphile complexes in the solid state and the conditions for formation of mesoscopic phases in flexible polymer chains. Paper III sums this work. It is based on small angle and wide angle scattering studies, infrared spectroscopy (FTIR) and theoretical estimates on the interaction energies. The authors responsibility has been the SAXS investigations which were made at HU.

The formation of the mesoscopic phases is observed to require a certain balance between the interaction strength and the length of the surfactant, longer surfactants requiring stronger interaction. Strong interaction such as protonation with strong acid [149] and complex coordination [150] have been shown to give mesophases; same conclusion can be drawn from alkyl phenols [151] provided that the alkyl length is between 12 and 22 carbon units. Less acidic groups such as fatty acids and aliphatic alcohols and amines do not provide sufficiently strong interaction and are either homogeneous or they phase separate macroscopically.

Paper IV. Paper IV studies in more detail one surfactant, PDP, from the alkylphenyl series. In this system, a sharp order-disorder transition (ODT) was observed [151]. In this work the ODT is surveyed at varying surfactant concentrations by simultaneous small angle, wide angle and calorimetry (DSC) measurements at the synchrotron facility of Daresbury, England. The transition was shown to be of first order and depend on the mole fraction of the surfactant.

Paper V. The final paper studies the same complex as in Paper IV, this time attached to a polystyrene (PS) block. The SAXS studies were performed at HU with both the conventional setup (as used above) and one that uses the longer distance of 1.2 m between the sample and the detector for studying the block polymer structure. The confinement of P4VP(PDP) in the block morphology was expected to affect its thermal phase behavior but this was not found to be the case. The phase diagram as a function of PS weigh fraction were obtained with transmission electron microscopy.

References

[1] B. Davis and C. M. Slack, *Phys.Rev.* **27** (1926) 796.

[2] B. Davis, *J.Franklin Inst.* **204** (1927) 29.

[3] V. I. Vaidyanathan, *Indian J.Phys.* **4** (1930) 501.; C. V. Raman and M. Ramanathan, *Proc.Ind.Assn.Cult.Sci.* **8** (1923) 129.

[4] S. H. Piper, *J.Chem.Soc.* **188** (1929) 414.

[5] P. Krishnamurti, *Indian J.Phys.* **3** (1928-29) 307.

[6] A. Guinier, *Compt.Rend.* **206** (1938) 1374.; A. Guinier, *Compt.Rend.* **206** (1938) 1641.; A. Guinier, *Ann.Phys.* **12** (1939) 161.

[7] G. Porod, *Kolloid-Z.* **124** (1951) 83.

[8] P. W. Schmidt, *J.Appl.Cryst.* **24** (1991) 414.

[9] O. Glatter and O. Kratky (Ed.), *Small-Angle X-ray Scattering*, Academic Press, London (1982).

[10] L. A. Feigin and D. I. Svergun, *Structure Analysis by Small-Angle X-ray and Neutron Scattering*, Plenum Press, New York (1987).

[11] G. R. Strobl, *Acta Cryst.* **A26** (1970) 367; O. Glatter and K. Gruber, *J.Appl.Cryst.* **26** (1993) 512.

[12] P. Alexandridis, U. Olsson and B. Lindman, *Langmuir* **14** (1998) 2627; P. Alexandridis, U. Olsson and B. Lindman, *Langmuir* **13** (1997) 23.

[13] R. W. James, *The Optical Principles of the Diffraction of X-rays*, G. Bell and Sons, London (1948).

[14] R. de L. Kronig and H. A. Kramers, *Z.Phys.* **48** (1928) 174.

[15] S. Brennan and P. L. Cowan, *Rev.Sci.Instrum.* **63** (1992) 850.

[16] G. Damaschun and J. Müller, *Z.Naturforsch.* **20** (1965) 1274.

[17] O. Kratky, *Makromol.Chem.* **35A** (1970) 12.

[18] L. B. Shaffer and W. W. Beeman, *J.Appl.Cryst.* **3** (1970) 379.

[19] R. W. Hendricks, P. G. Mardon and L. B. Shaffer, *J.Chem.Phys.* **61** (1974) 319.

[20] I. Piltz, *J.Coll.Interface Sci.* **30** (1969) 140.

[21] R. Perret and W. Ruland, *J.Appl.Cryst.* **5** (1972) 116.; N. J. Chonacky and W. W. Beeman, *Acta Cryst.* **A25** (1969) 564.

[22] P. Debye, *Ann. Physik* **46** (1915) 809.

[23] J.-P. Hansen and I. R. McDonald, *Theory of Simple Liquids*, Academic Press, London (1989).

[24] M. Born and H. S. Green, *Proc Roy.Soc.* **188** (1946) 10.

[25] J. G. Kirkwood, *J.Chem.Phys.* **3** (1935) 300.; J. G. Kirkwood and E. M. Boggs, *J.Chem.Phys.* **10** (1942) 394.

[26] J. G. Kirkwood, E. K. Maun and B. J. Alder, *J.Chem.Phys.* **18** (1950) 1040.

[27] H. S. Green, *Proc.Roy.Soc. A* **189** (1947) 103.

[28] A. E. Rodriguez, *Proc Roy.Soc.* **A196** (1949) 73.

[29] G. Fournet, *Acta Cryst.* **4** (1951) 293.

[30] L. S. Ornstein and F. Zernike, *Proc.Acad.Sci. Amsterdam* **17** (1914) 793.

[31] F. Zernike, *Proc.Acad.Sci. Amsterdam* **18** (1916) 1520.

[32] J.L. Lebowitz and J. K. Percus, *Phys.Rev.* **144** (1966) 251.

[33] E. Waisman, *Mol.Phys.* **25** (1973) 45.

[34] J. B. Hayter and J. Penfold, *Mol.Phys.* **42** (1981) 109.

[35] J.-P. Hansen and J. B. Hayter, *Mol.Phys.* **46** (1982) 651.

[36] J. K. Percus and G. J. Yevick, *Phys.Rev.* **110** (1958) 1.

[37] J. K. Percus, *Phys.Rev.Lett.* **8** (1962) 462.

[38] M. S. Wertheim, *Phys.Rev.Lett.* **10** (1963) 321.; E. Thiele, *J.Chem.Phys.* **39** (1963) 474.; M. S. Wertheim, *J.Math.Phys.* **5** (1964) 267.

[39] R. J. Baxter, *J.Chem.Phys.* **49** (1968) 2770.; R. J. Baxter, *Phys.Rev.* **154** (1967) 170.

[40] R. J. Baxter, *Aust.J.Phys.* **21** (1968) 563.; C. Regnaut and J. C. Ravey, *J.Chem.Phys.* **91** (1989) 1211.

[41] H. G. Duits, R. P. May, A. Vrij and C. G. de Kruif, *Langmuir* **7** (1991) 64.; D. Roux, A. M. Bellocq and M. S. Leblane, *Chem.Phys.Lett.* **94** (1983) 156.; S. V. G. Menon, V. K. Kelkar and C. Manohar, *Phys.Rev. A* **43** (1991) 1130.

[42] A. A. Broyles, *J.Chem.Phys.* **35** (1961) 493.; A. A. Khan and A. A. Broyles, *J.Chem.Phys.* **43** (1965) 43.; G. J. Throop and R. J. Bearman, *Physica* **32** (1966) 1298.; R. O. Watts, *J.Chem.Phys.* **48** (1968) 50.

[43] B. Barboy *J.Chem.Phys* **61** (1974) 3194.

[44] S. V. G. Menon, C. Manohar and K. Srinivasa Rao, *J.Chem.Phys.* **95** (1991) 9186.

[45] D. J. Kinning and E. L. Thomas, *Macromolecules* **17** (1984) 1712.

[46] J. L. Lebowitz, *Phys.Rev.* **133** (1964) 895.; J. L. Lebowitz and J. S. Rowlinson, *J.Chem.Phys.* **41** (1964) 133.; R. J. Baxter, *J.Chem.Phys.* **52** (1970) 4559.

[47] P. T. Cummings, J. W. Perram and E. R. Smith, *Mol.Phys.* **31** (1976) 535.; C. Robertus, W. H. Philipse, J. G. H. Joosten and Y. K. Levine, *J.Chem.Phys* **90** (1989) 4482.; B. Barboy *Chem.Phys* **11** (1975) 357.; L. Blum and G. Stell, *J.Chem.Phys.* **71** (1979) 42.; J. J. Salacuse and G. Stell, *J.Chem.Phys.* **77** (1982) 3714.; A. Vrij, *J.Chem.Phys.* **69** (1978) 1742.; A. Vrij, *J.Chem.Phys.* **71** (1979) 3267.; B. van Breuten and A. Vrij, *J.Chem.Phys.* **74** (1981) 2744.

[48] J. S. Rowlinson, *Mol.Phys.* **9** (1965) 217.; F. J. Rogers and D. A. Young, *Phys.Rev. A* **30** (1984) 999.; G. Zerah and J.-P. Hansen, *J.Chem.Phys* **84** (1986) 2336.

[49] J. Yvon, *Suppl.Nuevo Cimento* **9** (1958) 144.

[50] F. Mandel, *J.Chem.Phys.* **62** (1975) 1595.

[51] H. Takahashi, *Proc.Phys.Math.Soc.Japan* **24** (1942) 60.

[52] F. Gursey, *Proc. Cambridge Philos.Soc.* **46** (1950) 182.

[53] L. van Hove, *Physica* **XVI (2)** (1950) 137.

[54] L. Tonks, *Phys.Rev.* **50** (1936) 955.

[55] R. E. Peierls, *Proc.Cambridge Philos.Soc.* **32** (1934) 477.; L. D. Landau, *Phys.Z.Sowjetunion* **11** (1937) 26.

[56] L. D. Landau and E. M. Lifschitz, *Statistical Physics*, Pergamon Press, UK (1980) 432.

[57] M. Kac, *Phys.Fluids* **2** (1959) 8.; G. A. Baker, *Phys.Rev.* **122** (1961) 1477.; G. A. Baker, *Phys.Rev.* **126** (1962) 2071.

[58] F. Zernicke and J. A. Prins, *Z.Physik* **41** (1927) 184.

[59] R. Hosemann and S. N. Bagchi, *Direct Analysis od Diffraction by Matter* North Holland Publishing Co. (Groningen 1962).

[60] T. R. Welberry, G. H. Miller and C. E. Carroll, *Acta Cryst.* **A36** (1980) 921.

[61] J. N. Israelachvili, *Intermolecular and Surface Forces* Academic Press, San Diego (1992).

[62] B. Gallot and A. E. Skoulios, *Kolloid-Z. Z.Polymere* **208** (1966) 37.

[63] W. Z. Helfrich, *Naturforschung* **28** (1973) 693.

[64] D. A. Huse and S. Leibler, *J.Phys. (France)* **49** (1988) 605.

[65] S. A. Safran, L. A. Turkevich and P. A. Pincus, *J.Phys.Lett. (Paris)* **45** (1984) L69.; Z. G. Wang and S. A. Safran, *Europhys.Lett.* **11** (1990) 425.

[66] G. Gompper and M. Schick, *Self-Assembling Amphiphilic Systems*, Academic Press, UK (1994).

[67] T. A. Witten, *Rev.Mod.Phys.* **71** (1999) 367.

[68] M. Teubner and R. Strey, *J.Chem.Phys.* **87** (1987) 3195.

[69] P. Debye and A. M. Bueche, *J.Appl.Phys.* **20** (1949) 518.

[70] W. Helfrich, *Z.Naturforsch. A* **33a** (1978) 305.

[71] W. Janke and H. Kleinert, *Phys.Rev.Lett.* **58** (1987) 144.

[72] V. Luzzati and F. Husson, *J.Cell.Biol.* **12** (1962) 217.

[73] J. M. Vincent and A. Skoulios, *Acta Cryst.* **20** (1966) 432.

[74] P. A. Winsor, *Chem.Rev.* **68** (1968) 1.

[75] C. Madelmont and R. Perron, *Colloid.Polym.Sci* **254** (1976) 581.

[76] V. Luzzati, H. Mustacchi, A. Skoulios and F. Husson, *Acta Cryst.* **13** (1960) 660.

[77] P. A. Spegt, A. E. Skoulios and V. Luzzati, *Acta Cryst.* **14** (1961) 866.

[78] V. Luzzati and P. A. Spegt, *Nature* **215** (1967) 701.

[79] V. Luzzati, A. Tardieu, T. Gulik-Krzywicki, E. Rivas and F. Reiss-Husson, *Nature* **220** (1968) 485.

[80] F. Husson, H. Mustacchi and V. Luzzati, *Acta Cryst.* **13** (1960) 668.

[81] P. A. Spegt and A. E. Skoulios, *Acta Cryst.* **21** (1966) 892.

[82] V. Luzzati, T. Gulik-Krzywicki and A. Tardieu, *Nature* **218** (1968) 1031.

[83] V. Luzzati, A. Tardieu and T. Gulik-Krzywicki, *Nature* **217** (1968) 1028.

[84] L. E. Scriven, *Nature* **263** (1976) 123.

[85] A. H. Schoen, *NASA TN D-5541* Washington DC, (1970).

[86] K. Fontell, *Colloid.Polym.Sci* **268** (1990) 264.

[87] G. Lindblom and R. Rilfors, *Biochim.Biophys.Acta* **988** (1989) 221.

[88] W. Longley and T. J. McIntosh, *Nature* **303** (1983) 612.

[89] V. Luzzati, *J.Phys. II (France)* **5** (1995) 1649.

[90] G. Lindblom, K. Larsson, L. Johansson, K. Fontell and S. Forsen, *J.Am.Chem.Soc* **101** (1979) 5465-5470.

[91] K. Larsson, K. Fontell and N. Krog, *Chem.Phys.Lipids* **27** (1980) 321-8.

[92] B. Håkansson, P. Hansson, O. Regev and O. Söderman, *Langmuir* **14** (1998) 5730.

[93] S. M. Gruner, M. W. Tate, G. L. Kirk, P. T. C. So, D. C. Turner, D. T. Keane, C. P. S. Tilcock and P. R. Cullis, *Biochemistry* **27** (1988) 2853.

[94] R. H. Templer, J. M. Seddon, N. A. Warrender, A. Syrykh, Z. Huang, R. Winter and J. Erbes, *J.Phys.Chem. B* **102** (1998) 7251.

[95] R. Winter, J. Erbes, R. H. Templer, J. M. Seddon, A. Syrykh, N. A. Warrender and G. Rapp, *Phys.Chem.Chem.Phys.* **1** (1999) 887.

[96] J. L. Jones and T. C. B. McLeish, *Langmuir* **15** (1999) 7495-7503.

[97] S. Radiman, C. Topracioglu and A. R. Faruqi, *J.Phys. (Paris)* **51** (1990) 1501.

[98] R. R. Balmbra, J. S. Clunie and J. F. Goodman, *Nature* **222** (1969) 1159.

[99] A. Tardieu and V. Luzzati, *Biochim.Biophys.Acta* **219** (1970) 11.

[100] P. Mariani, V. Luzzati and H. Delacroix, *J.Mol.Biology* **204** (1988) 165.; P. Mariani, E. Rivas, V. Luzzati and H. Delacroix, *Biochemistry* **29** (1990) 6799.

[101] P-O. Eriksson, G. Lindblom and G. Arvidson, *J.Phys.Chem.* **89** (1985) 1050.; P-O. Eriksson, G. Lindblom and G. Arvidson, *J.Phys.Chem.* **91** (1987) 846.

[102] K. Fontell, K. K. Fox and E. Hansson, *Mol.Cryst.Liq.Cryst.* **1** (1985) 9.

[103] V. Luzzati, R. Vargas, A. Gulik, P. Mariani, J. M. Seddon and E. Rivas, *Biochemistry* **31** (1992) 279.

[104] J. Charvolin and J-F. Sadoc, *J.Physique* **49** (1988) 521.

[105] J. M. Seddon, *Biochemistry* **29** (1990) 7997; P. Alexandridis, U. Olsson and B. Lindeman, *Langmuir* **12** (1996) 1419.

[106] J. Als-Nielsen, J. D. Litster, R. J. Birgeneau, M. Kaplan, C. R. Safinya, A. Lindegaard-Endersen and S. Mathiesen, *Phys.Rev. B* **22** (1980) 312.

[107] L. Gunther, Y. Imry and J. Lajzerowicz, *Phys.Rev.A* **22** (1980) 1733.

[108] A. Caille and R. C. Seances, *Acad.Sci.Ser.B* **274** (1972) 871.

[109] C. R. Safinya, D. Roux, G. S. Smith, S. K. Sinha, P. Dimon, N. A. Clark and A. M. Bellocq, *Phys.Rev.Lett.* **57** (1986) 2718.

[110] F. Nallet, R. Laversanne and D. Roux, *J. Phys.II (France)* **3** (1993) 487.

[111] R. R. Balmbra, J. S. Clunie and J. F. Goodman, *Proc.Roy.Soc. A* **285** (1965) 534.

[112] J. Rogers and P. A. Winsor, *Nature* **216** (1967) 477.; P. A. Winsor, *Mol.Cryst.Liquid Cryst.* **12** (1971) 141.; K. Fontell, *J.Colloid Interface Sci.* **43** (1973) 156.

[113] P. Ekwall, L. Mandell and K. Fontell, *J.Colloid Interface Sci.* **33** (1970) 215.

[114] F. C. Larche, J. Appell, G. Porte, P. Bassereau and J. Marignan, *Phys.Rev.Lett.* **56** (1986) 1700.

[115] D. Roux and C. R. Safinya, *J.Phys. (France)* **49** (1988) 307.; F. Nallet, D. Roux and S. T. Milner, *J.Phys. (France)* **51** (1990) 2333.; T. Odijk, *Langmuir* **8** (1992) 1690.; R. J. de Vries, *Phys.Rev. E* **56** (1997) 1897.

[116] P. G. de Gennes, *The Physics of Liquid Crystals*, Oxford University Press, London (1974).

[117] J. V. Selinger and R. F. Bruinsma, *Phys.Rev. A* **43** (1991) 2910.

[118] T. Shimada, M. Doi and K. Okano, *J.Chem.Phys.* **88** (1988) 2815.

[119] P. van der Schoot and T. Odijk, *Macromolecules* **23** (1990) 4181.

[120] T. Neugebauer, *Ann.Phys.* **42** (1943) 509.

[121] J. F. Sadoc and J. Charvolin, *J.Phys. (Paris)* **47** (1986) 683.

[122] D. M. Anderson, S. M. Gruner and S. Leibler, *Proc.Natl.Acad.Sci. (USA)* **85** (1988) 5364.

[123] P. Kekicheff and G. J. T. Tiddy, *J.Phys.Chem.* **93** (1989) 2520.

[124] D. M. Anderson, H. T. Davis, L. E. Scriven and J. C. C. Nitsche, *Adv.Chem.Phys.* **77** (1990) 337.

[125] M. W. Tate and S. M. Gruner, *Biochemistry* **28** (1989) 4245.

[126] R. H. Templer, J. M. Seddon, P. M. Duesing, R. Winter and J. Erbes, *J.Phys.Chem. B* **102** (1998) 7262.

[127] S. T. Hyde, S. Andersson, B. Ericsson and K. Larsson, *Z.Kristallogr.* **168** (1984) 213.

[128] J. Charvolin, J. F. Sadoc, *J.Phys. (France)* **48** (1987) 1559.; J.-F. Sadoc and J. Charvolin, *Acta Cryst. A* **45** (1989) 10.; A. D. Benedicto and D. F. O'Brien, *Macromolecules* **30** (1994) 3395.

[129] A. Fogden and S. T. Hyde, *Eur.Phys.J. B* **7** (1999) 91.

[130] M. Clerc, Y. Hendrikx and B. Farago, *J.Phys.II (France)* **7** (1997) 1205.

[131] U. Olsson and K. Mortensen, *J.Phys.II (France)* **14** (1995) 789.

[132] P. Davidson, M. Impéror and A-M. Levelut, *SAS '99, XI_{th} International Conference on Small-Angle Scattering*, New York (1999).

[133] D. Siegel, *Chem.Phys.Lipids* **42** (1986) 279.

[134] Y. Rançon and J. Charvolin, *J.Phys.Chem.* **92** (1988) 2646.

[135] R. Kirste and G. Porod, *Kolloid Z.* **184** (1962) 1.

[136] M. A. Micha, C. Burger and M. Antonietti, *Macromolecules* **31** (1998) 5930.

[137] C. K. Ober and G. Wegner, *Adv.Mater.* **9** (1997) 17.

[138] P. L. Felger, T. R. Gadek, M. Holm, R. Roman, H. W. Chan, M. Wenz, J. P. Northrop, G. M. Ringold and M. Danielsen, *Proc.Natl.Acad.Sci. (USA)* **84** (1987) 7413.; N. Zhu, D. Liggitt, Y. Liu and R. Debs, *Science* **261** (1993) 209.; H. Gershon, R. Ghirlando, S. B. Guttman and A. Minsky, *Biochemistry* **32** (1993) 7143.; K. J. Crowell and P. M. Macdonald, *J.Phys.Chem. B* **101** (1997) 1105.; J. O. Rädler, I. Koltover, T. Salditt and C. R. Safinya, *Science* **275** (1997) 810.

[139] T. Tanaka, *Phys.Rev.Lett.* **40** (1978) 820.

[140] E. Sokolov, F. Yeh, A. Khokhlov, V. Ya. Grinberg and B. Chu, *J.Phys.Chem. B* **102** (1998) 7091.; S. Zhou, C. Burger, F. Yeh and B. Chu, *Macromolecules* **31** (1998) 8157.

[141] O. E. Filippova and S. G. Starodubtzev, *J.Polym.Sci.,Polym.Phys.Ed.* **31** (1993) 1471.

[142] K. Hayagawaand and J. C. Kwak, *J.Phys.Chem.* **86** (1982) 3866.; E. D. Goddard, *Colloids Surf.* **19** (1986) 301.; L. Piculell and B. Lindman, *Adv.Colloid Interface Sci.* **41** (1992) 149.; K. Thalberg and B. Lindman, *Interactions of Surfactants with Polymers and Proteins* E.D. Goddard and K. P. Ananthapadmanabhan Eds., CRC Press: Bocca Raton, FL (1993) 203.; P. Ilekti, L. Piculell, F. Tournilhac and B. Cabane *J.Phys.Chem. B* **102** (1998) 344.

[143] M. Antonietti, C. Burger and J. Effing, *Adv.Mater.* **7(8)** (1995) 751.; M. Antonietti, C. Burger and A. Thünemann, *Trends in Polym.Sci.* **5** (1997) 262.

[144] A. Harada and S. Nozakura, *Polym.Bull.* **11** (1984) 175.; M. Antonietti, J. Conrad and A. Thünemann, *Macromolecules* **27** (1994) 6007.; M. Antonietti and M. Maskos, *Macromol.Rapid Comm.* **16** (1995) 763.

[145] R. Goetz and W. Helfrich, *J.Phys.II.(France)* **6** (1996) 215.; M. Antonietti, M. Wenzel and A. Thünemann, *Langmuir* **12** (1996) 2111.

[146] M. Antonietti, M. Maskos, *Macromolecules* **29** (1996) 4199.

[147] M. Antonietti and J. Conrad, *Angew.Chem.Int.Ed.Engl.* **33** (1994) 1869.

[148] G. H. Fredrickson, *Macromolecules* **26** (1993) 2825.

[149] O. Ikkala, J. Ruokolainen, G. ten Brinke, M. Torkkeli and R. Serimaa, *Macromolecules* **28** (1995) 7088.

[150] J. Ruokolainen, J. Tanner, G. ten Brinke, O. Ikkala,, M. Torkkeli and R. Serimaa, *Macromolecules* **28** (1995) 7779.

[151] J. Ruokolainen, G. ten Brinke, O. Ikkala,, M. Torkkeli and R. Serimaa, *Macromolecules* **29** (1996) 3409.

[152] J. Ruokolainen, R. Mäkinen, M. Torkkeli, T. Mäkelä, R. Serimaa, G. ten Brinke and O. Ikkala, *Science* **280** (1998) 557.

[153] L. Leibler, *Macromolecules* **13** (1980) 1602.

[154] R. V. Tal'roze, S. A. Kuptsov, T. I. Sycheva, V. S. Bezbodorov and N. A. Plate, *Macromolecules* **28** (1995) 8689.

[155] J. Ruokolainen, M. Torkkeli, R. Serimaa, E. Komanschek, G. ten Brinke and O. Ikkala, *Macromolecules* **30** (1997) 2002.

[156] J.-M. Lehn, *Angew.Chem.,Int.Ed.Engl.* **29** (1990) 1304.; C. Fouquey, J.-M. Lehn and A.-M. Levelut, *Adv.Mater.* **2** (1990) 254.; P. Bladon and A. C. Griffin, *Macromolecules* **26** (1993) 6604.; C. Alexander, C. P. Jariwala, C. M. Lee and A. C. Griffin, *Macromol.Symp.* **77** (1994) 283.

[157] T. Kato and J. M. J. Fréchet, *Macromolecules* **22** (1989) 3818.; S. Ujiie and K. Iimura, *Chem.Lett.* (1991) 411.; S. Ujiie and K. Iimura, *Macromolecules* **25** (1992) 3174.; T. Kato, H Kihara, T. Uryu, A. Fujishima and J. M. J. Fréchet, *Macromolecules* **25** (1992) 6936.; U. Kumar, T. Kato and J. M. J. Fréchet, *J.Am.Chem.Soc.* **114** (1992) 6630.; U. Kumar, J. M. J. Fréchet, T. Kato, S. Ujiie and K. Iimura, *Angew.Chem.,Int.Ed.Engl.* **31** (1992) 1531.; U. Kumar, J. M. J. Fréchet, *Adv.Mater.* **4** (1992) 665.; C. G. Bazuin and F. A. Brandys, *Chem.Mater.* **4** (1992) 970.; R. V. Tal'roze and N. A. Platé, *Polymer Science* **36** (1994) 1479.; S. Malik, P. K. Dhal and R. A. Mashelkar, *Macromolecules* **28** (1995) 2159.;

[158] C. Sadron and B. Gallot, *Makromol.Chem.* **164** (1973) 301.

[159] S. L. Aggarwal, *Polymer* **17** (1976) 938.

[160] V. L. Ginzburg, *Sov.Phys.Solid State* **2** (1960) 1824.; K. Binder, *Phys.Rev. A* **29** (1984) 341.

[161] G. H. Fredrickson and E. Helfand, *J.Chem.Phys.* **87** (1987) 697.

[162] F. S. Bates, J. H. Rosedale and G. H. Fredrickson, *J.Chem.Phys.* **92** (1990) 6255.

[163] H. Hasegawa, H. Tanaka, K. Yamasaki and T. Hashimoto, *Macromolecules* **20** (1987) 1651. D. S. Herman, D. J. Kinning, E. L. Thomasand L. J. Fetters, *Macromolecules* **20** (1987) 2940.

[164] F. S. Bates, *Science* **251** (1991) 898.;

[165] J. H. Rosedale, F. S. Bates, K. Almdal, K. Mortensen and G. D. Wignall, *Macromolecules* **28** (1995) 1429.

[166] F. S. Bates, J. H. Rosedale, G. H. Fredrickson and C. J. Glinka, *Phys.Rev.Lett.* **61** (1988) 2229.; N. Sakamoto and T. Hashimoto, *Macromolecules* **28** (1995) 6825.; K. Mori, A. Okawara and T. Hashimoto, *J.Chem.Phys.* **104** (1996) 7765.

[167] K. Almdal, K. Mortensen, A. J. Ryan and F. S. Bates, *Macromolecules* **29** (1996) 5940.

[168] S.H. Mai, P. A. Fairclough, I. W. Hamley, M. W. Matsen, R. C. Denny, B.-X. Liao, C. Booth and A. J. Ryan, *Macromolecules* **29** (1996) 6212.

[169] S. P. Gido and Z.-G. Wang, *Macromolecules* **30** (1997) 6771.

[170] M. F. Schultz, A. K. Khandpur, F. S. Bates, K. Almdal. K. Mortensen, D. A. Hajduk and S. M. Gruner, *Macromolecules* **29** (1996) 2857-2867.; D. A. Hajduk, H. Takenouchi, M. A. Hillmyer, F. S. Bates, M. E. Vigild and K. Almdal, *Macromolecules* **30** (1997) 3788.

[171] K. Almdal, K. A. Koppi, F. S. Bates and K. Mortensen, *Macromolecules* **25** (1992) 1743.

[172] D. A. Hajduk, P. E. Harper, S. M. Gruner, C. C. Honeker, G. Kim, E. L. Thomas and L. J. Fetters, *Macromolecules* **27** (1994) 4063.

[173] A. N. Semenov, I. A. Nyrkova and A. R. Khokhlov, *Macromolecules* **28** (1995) 7491.

[174] C. Burger, M. A. Micha, S. Oestreich, S. Förster and M. Antonietti, *Europhys.Lett.* **42** (1998) 425.

[175] Y. Mogi, H. Kotsuji, Y. Kaneko, K. Mori, Y. Matsushita and I. Noda, *Macromolecules* **25** (1992) 5408.; Y. Mogi, K. Mori, Y. Matsushita and I. Noda, *Macromolecules* **25** (1992) 5412.; C. Auschra and R. Stadler, *Macromolecules* **26** (1993) 2171.; S. P. Gido, D. W. Schwark, E. L. Thomas and M. d. Carmo Gonąlves, *Macromolecules* **26** (1993) 2636.; R. Stadler, C. Aushra, J. Beckmann, U. Krappe, I. Voigt-Martin and L. Leibler, *Macromolecules* **28** (1995) 3080.; U. Krappe, R. Steidler and I. Voigt-Martin, *Macromolecules* **28** (1995) 4558.; W. Zheng and Z.-G. Wang, *Macromolecules* **28** (1995) 7215.; E. E. Dormidontova and A. R. Khoklov, *Macromolecules* **30** (1997) 1980.

[176] E. L. Thomas, D. B. Alward, D. J. Kinning, D. C. Martin, D. L. Handlin and L. J. Fetters, *Macromolecules* **19** (1986) 2197.

[177] D. A. Hajduk, P. E. Harper, S. M. Gruner, C. C. Honeker, E. L. Thomas and L. J. Fetters, *Macromolecules* **28** (1995) 2570.

[178] I. W. Hamley, *The Physics of Block Copolymers*, Oxford University Press, New York (1998).

[179] J. Ruokolainen, J. Tanner, O. Ikkala, G. ten Brinke and E. L. Thomas, *Macromolecules* **31** (1998) 3532.

[180] J. Ruokolainen, G. ten Brinke and O. Ikkala, *Adv.Mater.* **11** (1999) 777.

[181] J. W. Cahn, *J.Chem.Phys.* **42** (1965) 93.

[182] N. F. Berk, *Phys.Rev.Lett.* **58** (1987) 2718.

[183] T. Hashimoto, M. Shibayama and H. Kawai, *Macromolecules* **13** (1980) 1237.

[184] G. Hadziioannou, C. Picot, A. Skoulios. M.-L. Ionescu, A. Mathis, R. Duplessix, Y. Gallot and J.-P. Lingelser, *Macromolecules* **15** (1982) 263.; H. Hasegawa, T. Hashimoto, H. Kawai, T. P. Lodge, E. J. Amis, C. J. Glinka and C. C. Han, *Macromolecules* **18** (1985) 67.; N. Torikai, I. Noda, A. Karim, S. K. Satija, C. C. Han, Y. Matsushita and T. Kawakatsu, *Macromolecules* **30** (1997) 2907.; T. P. Lodge, M. W. Hamersky, K. J. Hanley and C.-I Huang, *Macromolecules* **30** (1997) 6139.

[185] J. T. Chen, E. L. Thomas, C. K. Ober and G.-P. Mao, *Science* **273** (1996) 343.

[186] H. Fisher and S. Poser, *Acta Polymer.* **47** (1996) 413.; G. Mao and C. K. Ober, *Acta Polymer.* **48** (1997) 405.; S. Poser, H. Fisher and M. Arnold, *Prog.Polym.Sci* **23** (1998) 1337.

[187] R. Mäkinen, J. Ruokolainen, O. Ikkala, K. de Moel, G. ten Brinke, W. de Ododrico and M. Stamm, *Macromolecules* **33** (2000) 3441.

[188] M. Yamada, T. Iguchi, A. Hirao, S. Nakahama and J. Watanabe, *Macromolecules* **28** (1997) 50-8.; H. Fisher, S. Poser and M Arnold, *Liquid Crystals* **18** (1995) 503.; G. Mao, J. Wang, S. R. Clingman, C. K. Ober, J. T. Chen and E. L. Thomas, *Macromolecules* **30** (1997) 2556.

[189] S. Hietala, S. Holmberg, M. Karjalainen, J. Näsman, M. Paronen, R. Serimaa, F. Sundholm and S. Vahvaselkä, *J.Mater.Chem.* **7** (1997) 721.; S. Hietala, S. Holmberg, J. Näsman, D. Ostrovskii, M. Paronen, R. Serimaa, F. Sundholm, L. Torell and M. Torkkeli, *Angew.Makromol.Chem.* **253** (1997) 151.; S. Hietala, M. Paronen, S. Holmberg, J. Näsman, J. Juhanoja, M. Karjalainen, R. Serimaa, M. Toivola, T. Lehtinen, K. Parovuori, G. Sundholm, H. Ericson, B. Mattsson, L. Torell and F. Sundholm, *J.Polym.Sci. Part A:Polym.Chem.*. **37** (1999) 1741.; M. Paronen, M. Karjalainen, K. Jokela, M. Torkkeli, R. Serimaa, J. Juhanoja, D. Ostrovskii, F. Sundholm, T. Lehtinen, G. Sundholm and L. Torell, *J.Appl.Polym.Sci.* **73** (1999) 1273.; K. Jokela, R. Serimaa, M. Torkkeli, M. Elomaa, F. Sundholm, N. Walsby, T. Kallio and G. Sundholm, *J.Appl.Cryst.* **33** (2000) 723.